SIAM J. Appl. Math.
Vol. 0, No. 0, pp. 000–000

RHYTHMOMIMETIC DRUG DELIVERY: MODELING, ANALYSIS, AND NUMERICAL SIMULATION*

LINGXING YAO†, M. CARME CALDERER‡, YOICHIRO MORI‡, AND RONALD A. SIEGEL§

Abstract. We develop, analyze, and numerically simulate a model of a prototype, glucose-driven, rhythmic drug delivery device, aimed at hormone therapies, and based on chemomechanical interaction in a polyelectrolyte gel membrane. The pH-driven interactions trigger volume phase transitions between the swollen and collapsed states of the gel. For a robust set of material parameters, we find a class of solutions of the governing system that oscillate between such states, and cause the membrane to rhythmically swell, allowing for transport of the drug, fuel, and reaction products across it, and collapse, hampering all transport across it. The frequency of the oscillations can be adjusted so that it matches the natural frequency of the hormone to be released. This work is linked to extensive laboratory experimental studies of the device built by Siegel's team. The thinness of the membrane and its clamped boundary, together with the homogeneously held conditions in the experimental apparatus, justify neglecting spatial dependence on the fields of the problem. Upon identifying the forces and energy relevant to the system, and taking into account its dissipative properties, we apply Rayleigh's variational principle to obtain the governing equations. The material assumptions guarantee the monotonicity of the system and lead to the existence of a three-dimensional limit cycle. By scaling and asymptotic analysis, this limit cycle is found to be related to a two-dimensional one that encodes the volume phase transitions of the model. The identification of the relevant parameter set of the model is aided by a Hopf bifurcation study of steady state solutions.

Key words. polyelectrolyte gel, volume transition, chemical reaction, hysteresis, weak solution, inertial manifold, limit cycle, competitive dynamical system, multiscale

AMS subject classifications. 34C12, 37G15, 74B20, 82B26, 94C45

DOI. 10.1137/16M1067007

1. Introduction.

In this paper, we model, analyze, and numerically simulate dynamical processes generated by an experimentally developed, one of a kind, drug delivery device, based on a polyelectrolyte gel membrane that swells and collapses in a glucose rich environment, in response to an enzyme-driven chemical reaction [6, 5, 26]. The gradient in pH between the membrane and its environment is the driving agent of the system.

The model consists of a competitive system of three ordinary differential equations describing the chemomechanical processes within the gel membrane and its interaction with other parts of the device, and with the environment. Out of the many material parameters of the model, the analysis identifies a special class $\mathcal{P}$ for which a robust oscillatory pattern of the system emerges. The work applies tools from the theory of dynamical systems to identifying physically meaningful invariant sets of initial data,

*Received by the editors March 22, 2016; accepted for publication (in revised form) January 11, 2017; published electronically DATE.
http://www.siam.org/journals/siap/x-x/M106700.html
Funding: The second author's work was supported by the National Science Foundation through the grants DMS-0909165 and DMS-GOALI-1009181. The fourth author's work was supported by the National Institutes of Health through grant HD040366.
†Department of Mathematics, Applied Mathematics and Statistics, Case Western Reserve University, Cleveland, OH 44106 (lingxing.yao@case.edu).
‡School of Mathematics, University of Minnesota, Minneapolis, MN 55455 (calde014@umn.edu, ymori@math.umn.edu).
§Departments of Pharmaceutics and Biomedical Engineering, University of Minnesota, Minneapolis, MN 55455 (siege017@umn.edu).

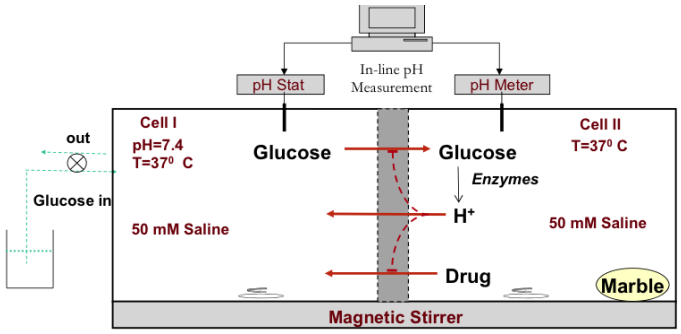

FIG. 1. *Experimental oscillator and schematic representation of the negative feedback structure* [6, 26].

analyzing time scales and their role in finding a relevant inertial manifold and the corresponding reduced two-dimensional system with its own invariant manifolds, determining their stability and that of the relevant stationary states, the ω-limit sets of the original and the reduced systems, carrying out numerical studies of Hopf bifurcation that yield relevant insight on the stability of periodic orbits, and establishing existence of limit cycles common to both systems.

A polyelectrolyte gel is an interactive mixture of polymer and fluid (water, in the case of a hydrogel), the latter containing several species of ions and the polymer including electrically charged (negative) side groups. Gels may experience phase transitions, triggered either by a gradient of temperature or pH, that change their permeability properties, from a collapsed, impermeable state to a fully permeable swollen one, capable of sustaining transport of molecules across it.

Research on drug delivery systems is focused on presenting the drug at the right place in the body at the right time [30]. While many existing devices aim at a continuous delivery over a time period, the one presented in this paper gives a prototype of a device operating in a rhythmic fashion. To this end, we have introduced a prototype chemomechanical oscillator that releases Gonadotropin-Releasing Hormone (GnRH) in rhythmic pulses, fueled by exposure to a constant level of glucose [6, 5, 26]. Experience with chemical and biochemical oscillators [13, 8, 12], and with electrical and mechanical relaxation oscillators [1], shows that rhythmic behavior can be driven by a constant rate stimulus, provided proper delay, memory, and feedback elements are employed in device dynamics. The device operates at the pH range of the human body.

The device shown in Figure 1 consists of two fluid compartments, an external cell (I) mimicking the physiological environment, and a closed chamber (II), separated from I by a hydrogel membrane. Cell II, containing the hormone drug to be delivered to the body, is the site of an enzyme reaction that converts glucose into hydrogen ions, and it also contains a piece of marble to remove excess hydrogen ions produced by an overactive reaction. These ions control the permeability properties of the membrane that, in its swollen state, allows for the transport of drug to the environment and facilitates the influx of glucose into the closed chamber. They also react with the swollen gel network and cause its collapse, providing a negative feedback by hampering the access to glucose whose chemical reaction generates them.

The hydrogel of the experimental device is a relatively thin membrane that is laterally restrained by clamping, justifying its treatment as a one-dimensional system,

with the polymer experiencing uniaxial deformations only. Moreover, the experimental apparatus is kept well-stirred at all times, allowing for further reduction to a time-dependent, spatially homogeneous system. The fields of the system include the thickness $L = L(t)$ (alternatively, the polymer volume fraction $\phi(t)$), the hydrogen concentrations $x(C_H^M)$ and $z(C_H^{II})$ inside the membrane, and in the chamber, respectively. The governing system also takes into account the algebraic constraint of electroneutrality.

A scaling analysis yields five dimensionless parameter groups $\mathcal{A}_i$ that encode most mechanical and chemical properties of the system. These together with control parameters, such as salt concentration C_{NaCl}, reaction rate constant of the marble k_{mar}, degree of ionization of the polymeric side groups σ_0, constant reference polymer volume fraction ϕ_0, and degree of polymer cross-linking ρ_0, are sufficient to fully describe the evolution properties of the system. Time scales associated with $\mathcal{A}_i$ reveal a dimensionless time constant of the order of 10^{-5} associated with membrane swelling, and time constants of magnitude 10^{-2} and 1 for changes of hydrogen ion concentrations in the reaction chamber and in the gel membrane, respectively. We will employ the virginal time notation t and τ to denote the *fast* and *slow* time variables, respectively. Changes in glucose and salt concentration take place several orders of magnitude faster than changes in the swelling ratio and so justify taking such concentration values as uniform in all parts of the device.

Although the original system has positive C^1-solutions, with ϕ bounded away from 0 and 1, and the concentration variables x and z bounded away from 0, its two-dimensional restriction to the nullcline, invariant manifold $\mathcal{N}$, involves multivalued functions that define the invariant submanifolds, $\mathcal{M}$ and $\mathcal{M}^-$, with $\mathcal{N} = \mathcal{M} \cup \mathcal{M}^-$, that serve as tools to investigate stability properties of solutions of the three-dimensional system. The dynamics in $\mathcal{M}$ takes place in the slower time τ, whereas solutions in $\mathcal{M}^-$ evolve according to t. $\mathcal{N}$ also turns out to be a global attractor of the whole system. From a different point of view, the two-dimensional system restricted to $\mathcal{M}$ admits weak solutions that precisely capture the hysteresis behavior of the problem. These are also effective solutions, from the point of view that changes occurring in the fast time scale are replaced by discontinuities in ϕ, in accordance with the volume phase transition behavior.

A study of the stationary states and their numerical Hopf bifurcation leads to the characterization of a parameter region $\mathcal{P}$, for which hysteretic and oscillatory behaviors occur, these being fully validated by laboratory experiments [3, 10, 2]. With each set of parameters in the region $\mathcal{P}$, determined by two Hopf bifurcation curves, there is associated a unique hyperbolic steady state, and a stable limit cycle belonging to $\mathcal{M}$. The latter, established by the Poincaré–Bendixon theorem for plane systems, also turns out to be the ω-limit set of positive semiorbits of the full system. Finally, applying the theory of competitive three-dimensional systems, we conclude that such a ω-limit set is also a limit cycle of the original system. It turns out that our system is qualitatively analogous to that modeling the dynamics of HIV in the regime where the concentrations of infected and uninfected T-cells and the virus follow a periodic holding pattern, away from the fully infected state represented by a hyperbolic steady state [23].

The outline of this paper is as follows. In section 2, we describe the prototype oscillator and outline its basis for operation. In section 3, we study the mechanical and chemical properties of the system. The assumptions of the model and the subsequent formulation of a precursory system of ordinary differential equations are presented in section 4. In section 5, we describe the parameters of the system and explore

its scaling properties and time scales, from which the system of ordinary differential equations that model the dynamics of the oscillator follows. We establish boundedness properties of the solutions, ensuring that solutions will remain in the physically meaningful regimes for all time. These are also essential in determining long time and stability properties of the system. The Hopf bifurcation analysis of the unique hyperbolic equilibrium point is presented in section 6. In section 7, we construct an inertial manifold $\mathcal{N}$ of the three-dimensional system and its submanifolds $\mathcal{M}$ and $\mathcal{M}^-$ and analyze the corresponding two-dimensional flow in these manifolds, demonstrating existence of an asymptotically stable limit cycle. We construct the hysteretic, weak solutions of the system that evolve in $\mathcal{M}$. In section 8, we study the monotonicity properties of the system and prove the existence of a three-dimensional limit cycle. We conclude with a discussion of the benefits and deficiencies of the present model.

2. Rhythmic hormone delivery: A simple experimental system. A simplified schematic representation of the experimental oscillator is depicted in Figure 1 [6, 26]. The apparatus consists of two well-stirred fluid compartments, or cells, separated by a swellable hydrogel membrane. Cell I, which is meant to mimic the external physiological fluid environment, contains glucose in saline solution, with fixed glucose concentration maintained by introduction of fresh medium and removal of reaction products by flow, and fixed pH 7.0 enforced by a pH-stat servo (autotitrating burette). Cell II, which simulates the interior of the rhythmic delivery device, contains the hormone to be released (e.g., GnRH) and the enzymes glucose oxidase, catalase, and gluconolactonase, which catalyze conversion of glucose to gluconic acid. The latter rapidly dissociates into hydrogen ion (H^+) and gluconate ion:

$$\text{Glucose} + O_2 \overset{enzymes}{\longrightarrow} H^+ + \text{Gluconate}^- + \frac{1}{2}O_2 \text{ (I)}.$$

Cell II also contains physiologic saline, which is exchanged with Cell I through the membrane, and a piece of solid marble. Marble is solid calcium carbonate, $CaCO_3(s)$, which reacts with H^+ according to

$$2H^+ + CaCO_3(s) \longrightarrow Ca^{2+} + CO_2\uparrow + H_2O \text{ (II)}.$$

The hydrogel membrane is clamped between Cells I and II. The degree of swelling of the membrane and permeabilities to glucose and GnRH depend on the internal concentration of H^+ ions, through the reaction [7, 14, 29]

$$\vdash COO^- + H^+ \rightleftharpoons \vdash COOH \text{ (III)}.$$

At low H^+ concentration, the membrane is charged, swollen, and highly permeable to both glucose and GnRH, but permeability to these compounds is substantially attenuated at higher H^+ concentrations where the membrane has less charge and is relatively collapsed. The placement of the membrane between a source of fuel, glucose, and its converting enzymes creates a dynamic environment with competing effects. On the one hand, the enzyme reaction produces H^+, which affects the permeability of the membrane; it is removed from the system by reacting with marble, and also by diffusing out to the environment. This creates a negative feedback mechanism between the enzyme reaction and the membrane permeability to glucose. Under proper conditions, this arrangement can lead to oscillations.

When the membrane is ionized and swollen, glucose permeates from Cell I to Cell II and is converted to H^+, which diffuses back into the membrane, binds and neutralizes the $\vdash COO^-$ groups, and causes the hydrogel membrane to collapse. The

membrane is now impermeable to glucose, and enzymatic production of H^+ is attenuated. Eventually, the H^+ ions bound to the membrane and diffuse into Cell I, where they are neutralized by the pH-stat and removed in the waste stream. The membrane then reionizes and reswells, and the system is primed to repeat the previous sequence of events.

In order to achieve sustained oscillations, a steady state in which flux of glucose, enzyme reaction rate, and flux of H^+ are balanced and equal at all times must be avoided. As will be seen, bistability, or hysteresis of membrane swelling response to H^+, provides a means for destabilizing such a steady state.

The reader is referred to experimental details and results in previous publications [6, 5, 26].

3. A lumped parameter model. A full mathematical description of the experimental system just described would require a detailed account of (1) diffusional and convective fluxes of solvent and solutes, (2) the spatial three-dimensional mechanics of the hydrogel membrane which, though constrained by clamps, exhibits swelling and shrinking which is both time and position dependent, (3) the kinetics of enzymatic conversion of glucose to H^+, and (4) the kinetics of binding and dissociation of H^+ with $\vdash COO^-$ groups. An accurate, verifiable model of this sort, which would require partial differential equations to describe intramembrane processes, does not yet exist. Here we simplify the problem by assuming that the membrane is a lumped, uniform element. All mechanical and chemical variables are homogenized to single values representing the whole membrane. We recognize that some potentially important consistencies are lost in this approximation. First, there will always be a difference in pH between Cells I and II, which will lead to intramembrane gradients in the chemical and mechanical variables. Second, self-consistent boundary conditions, which would follow naturally from a PDE model, must be replaced by somewhat ad hoc assumptions.

As a second simplification, we assume that the enzyme reactions, and the process of distribution of the dominant background electrolyte, NaCl, between Cells I and II and the hydrogel membrane, are very fast compared to the other dynamical processes. These assumptions can be justified, respectively, by the excess of enzyme used in the experiments, and the fact that the capacity of the membrane for acidic protons (H^+, or $\vdash COOH$) relative to Cells I and II far exceeds its relative capacities for Na^+ and Cl^-. Many experimental studies with polyacidic hydrogels have confirmed that H^+ dynamics and poroelastic relaxations are much slower than those of NaCl [3, 2, 10].

3.1. Swelling of hydrogels. The membranes considered in this work are crosslinked networks of polymer chains, or hydrogels, which absorb substantial amounts of water. Depending on water content, or degree of swelling, the hydrogel will be more or less permeable to solutes such as glucose and H^+. Hydrogels have a long history of application in drug delivery and medicine due to their mechanical and chemical compatibility with biological tissues and their ability to store and release drugs in response to environmental cues [28].

In the present system, we utilize the hydrogen ions H^+ that are enzymatically generated from glucose to control hydrogel swelling and hence release of hormone. In polyacid hydrogels, swelling is controlled by degree of ionization, which results from dissociation of acidic side groups that are attached to the polymer chains. When NaCl is present in the aqueous fraction of the hydrogel, the ionization equilibrium is

represented by

$$\vdash \mathrm{COOH} + \ \mathrm{Na}^+ + \mathrm{Cl}^- \rightleftharpoons \vdash \mathrm{COO}^- \ \mathrm{Na}^+ + \mathrm{H}^+ + \mathrm{Cl}^-.$$

Swelling of a polyacidic hydrogel results from three thermodynamic driving forces [7, 11, 20, 29]. First, there is the tendency of solvent (water) to enter the hydrogel and mix with polymer in order to increase translational entropy. The mixing force also depends on the relative molecular affinity or aversion of the polymer for water compared to itself due to short range van der Waals, hydrogen bonding, and hydrophobic interactions. Second, there is an elastic force, which is a response to the change in conformational entropy of the polymer chains that occurs during swelling or shrinking. The third force is due to ionization of the acidic pendant groups, which leads to an excess of mobile counterions and salt inside the hydrogel compared to the external medium, promoting osmotic water flow into the hydrogel. The ion osmotic force acts over a much longer range than the direct polymer/water interaction.

In the present work, it is assumed that the hydrogel is uniform in composition when it is prepared. The hydrogel at preparation is taken as the reference state for subsequent thermodynamic model calculations. At preparation, the volume fraction of polymer in the hydrogel is denoted by ϕ_0. Crosslinking leads to an initial density of elastically active chains, ρ_0. The initial density of ionizable acid groups, fixed to the polymer chains, is denoted by σ_0. Both densities have units mol/L and are referred to the total volume of the hydrogel (polymer+water) at preparation.

3.2. Mechanics of swelling. Since the hydrogel membrane used in the experiments is relatively thin and laterally restrained by clamping, we assume that the main swelling effect occurs along the thickness direction, so that the deformations sustained by the membrane are uniaxial. The swelling state of a hydrogel is then characterized by the volume fraction ϕ of the polymer at time $t > 0$. Letting the constants $0 < \phi_0 < 1$ and $L_0 > 0$ denote the volume fraction of polymer and the thickness of the membrane, respectively, in the reference state, the equation of conservation of mass of polymer in the gel is

$$L\phi = L_0\phi_0, \tag{1}$$

where $L = L(t)$ represents the membrane thickness at time $t > 0$, and $\alpha := \frac{\phi_0}{\phi}$ the elongation rate. In the model presented below, the three swelling forces, mixing, elastic, and ionic, yield the uniaxial swelling stress,

$$s = s_{\,\mathrm{mix}} + s_{\,\mathrm{elast}} + s_{\,\mathrm{ion}}\,, \tag{2}$$

which reflects the excess free energy density of the hydrogel relative to equilibrium, at a given state of swelling in a prescribed aqueous medium. At equilibrium, $s = 0$. Let $g_{\,\mathrm{mix}}$ and g_{elast} denote the Flory–Huggins mixing and elastic energy densities with respect to deformed volume, respectively. The corresponding total energy quantities, per unit cross-sectional area, are

$$G_{\mathrm{mix}} = Lg_{\,\mathrm{mix}}\,(\phi), \quad G_{\mathrm{elast}} = Lg_{\mathrm{elast}}(\phi). \tag{3}$$

A standard variational argument gives the dimensionless stress components as

$$s_{\,\mathrm{mix}} = -\frac{dG_{\mathrm{mix}}}{dL}, \quad s_{\,\mathrm{elast}} = -\frac{dG_{\mathrm{elast}}}{dL}. \tag{4}$$

Consequently,

$$s_i = -\left(g_i - \phi\frac{\partial g_i}{\partial \phi}\right), \quad i = \text{mix, elast.} \tag{5}$$

The mixing free energy density of solvent (water) with the hydrogel chains is modeled according to the Flory–Huggins expression

$$g_{\text{mix}} = \frac{RT}{v_{\text{w}}}[(1-\phi)\ln(1-\phi) + \chi\phi(1-\phi)], \tag{6}$$

where R is the gas constant, T is absolute (Kelvin) temperature, and v_{w} is the molar volume of water. The first term in the square brackets accounts for the translational entropy change of solvent molecules as they move from the external environment into the hydrogel, temporarily assuming that the bath is pure solvent. The second term accounts for short range contact interactions between polymer and solvent, summarized by the dimensionless parameter χ, which is the molar free energy required to form solvent/polymer contacts, normalized by RT. Introducing (6) into (5) yields

$$s_{\text{mix}} = -\frac{RT}{v_{\text{w}}}[\ln(1-\phi) + \phi + \chi\phi^2]. \tag{7}$$

In the simplest form of Flory–Huggins theory χ is constant, but in many hydrogel systems, especially those that undergo sharp swelling/shrinking transitions, a pseudo-virial series in ϕ is used. In the present work the series is truncated at the linear term, taking the form [9, 16]

$$\chi = \chi_1 + \chi_2\phi. \tag{8}$$

With $\chi_2 > 0$, polymer and solvent become increasingly incompatible as polymer concentration increases, with hydrogel shrinking and mixing pressure decreasing. Assuming that the polymer is a Neo–Hookean elastic solid, its uniaxial energy density and elastic stress, respectively, are

$$g_{\text{elast}} = RT\rho_0\Big(\frac{\phi}{\phi_0}\Big)\Big[\Big(\frac{\phi_0}{\phi}\Big)^2 - \ln\frac{\phi_0}{\phi} - 1\Big], \tag{9}$$

$$s_{\text{elast}} = -RT\rho_0\Big(\frac{\phi_0}{\phi} - \frac{\phi}{2\phi_0}\Big), \tag{10}$$

with the latter following from (5). The logarithmic term accounts for change in entropy of localization of crosslinks in the hydrogel due to swelling. The sum of (7) and (10) gives the Flory–Rehner stress, the nonionic component of the swelling stress established later. We now derive the evolution equation of the membrane according to the minimum rate of dissipation principle.

PROPOSITION 3.1. *Suppose that $\phi = \phi(t)$ and $L = L(t)$, $t \geq 0$, satisfy* (1). *Let us define the rate of dissipation function and the total energy as*

$$W = \frac{K}{2}\Big(\frac{dL}{dt}\Big)^2 \quad \textit{and} \quad E = G_{mix} + G_{elast}, \tag{11}$$

respectively, with $K > 0$ denoting a friction coefficient. Then the function $v = \frac{dL}{dt}$ that minimizes the Rayleighian functional $R = \dot{E} + W$, among spatially homogeneous fields, satisfies the equation

$$s_{mix} + s_{elast} - K\frac{dL}{dt} = 0, \tag{12}$$

with s_{mix} and s_{elast} as in (7) *and* (10), *respectively, and G_{elast} and G_{mix} as in* (3).

The proof results from the simple calculation

$$\frac{dE}{dt} = \frac{d}{dt}\big(g_{\text{mix}} + g_{\text{elast}}\big) = -(s_{\text{mix}} + s_{\text{elast}})v, \quad v = \frac{dL}{dt}. \tag{13}$$

So, the critical points $v = v(t)$ of R satisfy (12) for all $t \geq 0$. Defining the *permeability coefficient* as $K_{\text{w}} = \frac{RT}{K\nu_w}$, and using (7) and (10), we see that (12) becomes

$$\frac{dL}{dt} = -K_w\Big[\ln(1-\phi) + \phi + \chi\phi^2 + \nu_w\rho_0\Big(\frac{\phi_0}{\phi} - \frac{\phi}{2\phi_0}\Big)\Big]. \tag{14}$$

Equation (12) should be expanded to include the force s_{ion} as in (2), whose calculation is given next.

3.3. Chemical reactions. While the mixing and elastic terms represent important contributions to swelling pressure, the ionic term responds to H^+ concentration inside the membrane, and this is what forms the basis for the oscillator's dynamic behavior. As described above, ionization of the hydrogel occurs by dissociation of pendant carboxylic acid groups. The fraction of these groups that are ionized, f, is modeled according to a Langmuir isotherm relation,

$$f = \frac{K_{\text{A}}}{K_{\text{A}} + C_{\text{H}}}, \tag{15}$$

where C_{H} is the concentration of H^+ in the aqueous portion of the hydrogel and K_A is the dissociation constant of the carboxylic acid. The concentration of ionized groups, referenced to the aqueous portion of the hydrogel, is then given by

$$C_{\text{A-}} = f\sigma_0(\phi/\phi_0), \tag{16}$$

where σ_0 denotes the reference density of ionized groups fixed to the polymer chains. Letting C_{AH} denote the concentration of H^+ linked to carboxyl groups, the conservation of intramembrane hydrogen ions is given by the equation

$$L(C_{\text{H}} + C_{\text{AH}}) = L_0\sigma_0. \tag{17}$$

Combining (16) and (17) yields

$$C_{\text{AH}} = \frac{\phi}{\phi_0}(1-f)\sigma_0. \tag{18}$$

Ionization of hydrogel side-chains, plus the requirement for quasi-electroneutrality over any distance exceeding a few Debye lengths (~ 5 nm in physiological systems), leads to a distribution of mobile ions in the hydrogel that differs from that in the external bath. Ignoring very small contributions from H^+ and OH^- ions, a quasi-neutrality condition is

$$C_{\text{Na}} - C_{\text{Cl}} - C_{\text{A-}} = 0, \tag{19}$$

where C_{Na} and C_{Cl} are the concentrations, respectively, of Na^+ and Cl^- in the aqueous portion of the hydrogel.

For simplicity, we assume that Cells I and II contain fully dissociated NaCl, with ion concentrations $C'_{\text{Na}} = C'_{\text{Cl}} = C'_{\text{NaCl}}$. Ionic swelling stress in the membrane is modeled using van't Hoff's ideal law:

$$s_{\text{ion}} = RT(C_{\text{Na}} + C_{\text{Cl}} - 2C'_{\text{NaCl}}). \tag{20}$$

Derivation of this term from a free energy density expression is possible but not carried out here since the basis for van't Hoff's law is well understood.

It can be shown that diffusion of salt inside the hydrogel is very fast compared to diffusion of H+, which is retarded by reversible binding to pendant carboxylate groups [14], and to mechanical relaxation of swelling pressure. We may, therefore, assume that at any point in the hydrogel a Donnan quasi-equilibrium, where $C_{\text{Na}} = \lambda C'_{\text{Na}}$ and $C_{\text{Cl}} = \lambda^{-1} C'_{\text{Cl}}$, with λ the Donnan ratio, is determined by combining (15)–(19), giving

$$(1-\phi)\Big(\lambda - \frac{1}{\lambda}\Big)C'_{\text{NaCl}} - \sigma_0(\phi/\phi_0)f = 0. \tag{21}$$

With λ in hand, (20) becomes

$$s_{\text{ion}} = RT\left(\lambda + \frac{1}{\lambda} - 2\right)C'_{\text{NaCl}}. \tag{22}$$

Introducing (7), (8), (10), and (22) into (2) gives

$$\frac{v_{\text{w}} s}{RT} = -[\ln(1-\phi)+\phi+(\chi_1+\chi_2\phi)\phi^2] - v_{\text{w}}\rho_0\left(\frac{\phi_0}{\phi} - \frac{\phi}{2\phi_0}\right) + \left(\lambda + \frac{1}{\lambda} - 2\right)v_{\text{w}}C'_{\text{NaCl}}, \tag{23}$$

which, combined with (21), determines the total swelling stress. Rewriting (14) and taking the total stress into account leads to the force balance equation stated in (25).

Because (23) and (21) include elements of Flory–Rehner theory and Donnan and Langmuir quasi-equilibria, we call these two equations the FRDL model for uniaxial swelling stress. The behavior of this model depends on the hydrogel parameters ϕ_0, ρ_0, σ_0, χ_1, χ_2, and pK_{A}, and the external salt concentration C'_{NaCl}, which is assumed to be constant. These, together with relevant dimensionless parameter groups, determine the swelling and permeability properties of the hydrogel membrane.

3.4. Swelling equilibria. Before pursuing dynamics, it is useful to examine homogeneous uniaxial swelling equilibria for a hydrogel in a bath of fixed $pH = -\log C'_{\text{H}}$. In this case, $s = 0$ in (23) and $C_{\text{H}} = \lambda C'_{\text{H}} = \lambda 10^{-pH}$. Setting $pK_{\text{A}} := -\log K_{\text{A}}$, (21) becomes

$$\begin{aligned} &10^{-(pH-pK_{\text{A}})}(1-\phi)C'_{\text{NaCl}}\lambda^3 + (1-\phi)C'_{\text{NaCl}}\lambda^2 - \Big[10^{-(pH-pK_{\text{A}})}(1-\phi)C'_{\text{NaCl}} \\ &\qquad +\sigma_0\left(\frac{\phi}{\phi_0}\right)\Big]\lambda - (1-\phi)C'_{\text{NaCl}} = 0. \end{aligned} \tag{24}$$

We discuss the solvability of (24) with respect to λ. Since the physical parameters contributing to the polynomial coefficients are positive and $\phi \le 1$, there is only one sign change in the descending polynomial coefficients, and Descartes' rule of signs mandates a single positive real root. (Negative or complex values of λ are physically meaningless as they would predict negative or complex ion concentrations inside the hydrogel.) Moreover, substituting $\lambda = \nu + 1$ into (24) and rearranging terms, we obtain a cubic polynomial in ν that also has only one sign change; hence $\nu \ge 0$ and $\lambda \ge 1$. This makes physical sense, since for negatively charged hydrogel the internal cation concentration must exceed its external counterpart.

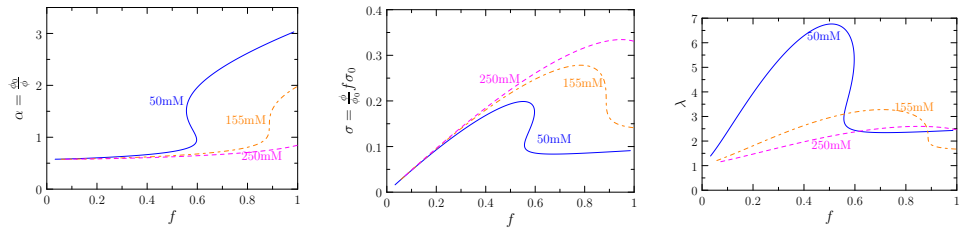

FIG. 2. *Figures* (a), (b), *and* (c) *show the* uniaxial swelling ratio α, *the* fixed charge density σ, *and the* Donnan ratio λ, *respectively, versus* ionized fraction f, *for different salt concentrations.*

The first and third terms of (24) can vary over several orders of magnitude with pH, indicating that pH, which affects ionization, will have a strong influence on salt ion partitioning and hence ion swelling pressure. When $pH \ll pK_{\rm A}$, the polymer is uncharged, $f \to 0$ and $\lambda \to 1$, and swelling takes on a minimum value determined by the mixing and elastic stresses. When $pH \gg pK_{\rm A}$, all acid groups are ionized with $f \to 1$, and swelling is maximal with λ substantially greater than 1.

Figure 2(a) displays the effect of ionized fraction f on uniaxial swelling ratio $\alpha{=}\chi_1 = 0.48$, $\chi_2 = 0.60$. This figure was generated using (23) with $s = 0$ and a version of (21).

As expected, swelling increases with decreasing salt concentration. For $C'_{\rm NaCl} =$ 250mM, the membrane remains in its essentially collapsed state with $\alpha < 1$. In this case hydrophobicity is the dominant force, and the effect of ion osmotic stress is relatively weak. For $C'_{\rm NaCl} =$ 155mM and 50mM, an initially shallow relation between α and f is punctuated by a rather sharp rise, indicating initial dominance of hydrophobicity that is overcome by ion osmotic stress at higher f. As ionic strength (salt concentration) decreases, the sharp rise occurs at lower ionization degree.

For $C'_{\rm NaCl} =$ 250mM and 155mM, f uniquely determines α. For $C'_{\rm NaCl} =$ 50mM, however, a range of bistability and hysteresis is observed. Over this range in f, total stress s vanishes at three values of α, corresponding to two free energy minima and one maximum in between. The latter, which corresponds to the negative slope branch of the swelling curve between the turning points, is unstable and need not be considered in the discussion of equilibria. Figure 2(b) shows the fixed charge density, $\sigma = (\phi/\phi_0) f\sigma_0$, as a function of f for the three salt concentrations. In all cases, this quantity initially rises with increasing f, since f is increasing but swelling does not change significantly. The rise is followed by a drop attributed to the sudden increase in swelling. Bistability is observed for $C'_{\rm NaCl} =$ 50mM over the same interval of f as before.

Figure 2(c) exhibits the calculated Donnan ratio λ as a function of f for the three salt concentrations. While these ratios provide information regarding the ion osmotic swelling force via (22), they also provide a link between external and internal pH. The curves are all nonmonotonic, with bistability for $C'_{\rm NaCl} =$ 50mM. The swings in λ more or less follow those of σ and can be explained in essentially the same way.

Figure 3 displays the relationship between pH and swelling for the three salt concentrations, considering both internal and external pHs (dotted and continuous lines, respectively). These values are determined according to (21) and (23), with $s = 0$, and $pH(\text{int}) = -\log C_{\rm H}$ and $pH(\text{ext}) = pH(\text{int}) + \log\lambda$. Evidently, increasing

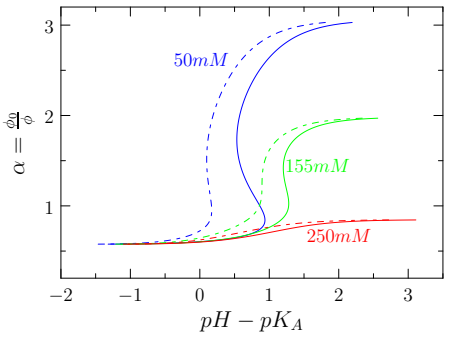

FIG. 3. *Swelling ratio α versus $pH - pK_A$ at different salt concentrations.*

salt concentration leads to an alkaline shift (higher pH) at which the major transition in swelling occurs. With increasing salt, a larger degree of ionization, and hence higher pH, is needed to effect the transition. The three pairs of graphs exhibit qualitatively different behaviors. For $C'_{\text{NaCl}} = 250$mM, both curves are monotonic and single valued, although internal pH is clearly lower than external pH, as expected based on Donnan partitioning of hydrogen ion. For $C'_{\text{NaCl}} = 50mM$, both curves exhibit bistability. At the intermediate salt concentration, $C'_{\text{NaCl}} = 155$mM, the internal pH curve is single valued, while the external pH curve shows bistability. This difference can be attributed to the Donnan effect, which nudges external pH to higher values at low degrees of ionization and swelling. Of course, the real control variable is external pH.

We conclude that there are two potential mechanisms underlying bistability, one originating from the relation between fixed charge density and degree of swelling, and the other stemming from the Donnan effect. While in these studies we looked at qualitative behaviors as a function of C'_{NaCl}, these behaviors might also be observed by altering structural parameters of the hydrogel. To simplify the notation, from now on, we will remove the "prime" symbol from the external salt concentration variable C'_{NaCl} and will write C_{NaCl} instead.

4. Spatially homogeneous chemomechanical model. Now that the axially restricted equilibrium swelling properties of the hydrogel membrane have been explored, we introduce a lumped parameter model of the chemomechanical oscillator illustrated in Figure 1. Variants of this model have been presented previously [6, 5]. The dynamic model is based on the following assumptions:

a. Membrane properties, including the fixed charge concentration, swelling state, and ion concentrations inside the membrane are assumed to be homogeneous in space. Upon suppressing lateral swelling and shrinking, the swelling state of the membrane is determined by its thickness $L = L(t)$. This homogeneity assumption is made even though the membrane is subjected to a pH gradient. External pH is homogenized by averaging the constant H^+ concentration in Cell I, C_H^I, and the variable H^+ concentration in Cell II, C_H^{II}; that is, $pH = \log[(C_H^I + C_H^{II})/2]$.

b. Chemical potentials inside the membrane are determined by the one-dimensional FRDL equation of state for one-dimensional swelling, as described above. From these, the total swelling stress, including the elastic, mixing, and ionic contributions, is given by (23), with λ determined according to the electroneutrality condition (21). Electroneutrality is enforced by rapid exchange of Na^+ and Cl^- between the membrane and Cells I and II. NaCl concentrations in Cells I and II are assumed constant and

equal [16].

c. Enzymatic conversion of glucose to gluconic acid is assumed to be instantaneous. This assumption is valid when the concentration of enzyme in Cell II is sufficiently high that transport of glucose into Cell II is rate limiting. Also, gluconate and bicarbonate, produced according to chemical reactions I and II, respectively, are presumed to not perturb the system's dynamics. The latter assumption is expected to hold best during early oscillations.

d. The rate of change of fixed, negative charge concentration is controlled by the rate of transport of hydrogen ions, which reversibly bind to pendant carboxylates as they diffuse through the membrane [14].

e. Permeability of the membrane to glucose is expressed as $K_{\mathrm{G}}^{0} e^{-\beta\phi}$, as suggested by free volume theory [33, 34]. The parameters K_{G}^{0} and β represent the hypothetical permeability with vanishing polymer concentration, and the sieving effect of the polymer, respectively, which depends on both polymer chain diameter and radius of the diffusant (glucose in this case). For hydrogen ions or water, which are much smaller than glucose, the sieving factor is assumed to be negligible, and we simply multiply the respective permeability coefficients, K_{h} and K_{w}, by $1-\phi$ to account for the aqueous space in the hydrogel that is available for transport of solutes.

Remark 4.1. In this model, diffusion of Na^+ and Cl^- are regarded as instantaneous, while diffusion of H^+ is regarded as rate determining, even though the diffusion coefficient of H^+ is decidedly larger. This assumption is justified in part due to the reversible binding of H^+ to the pendant carboxylates, which does not occur with Na^+ and Cl^-, and partly due to the very low H^+ concentration, which qualifies it for minority carrier status. Changes in concentration of H^+ in the membrane are rapidly buffered by readjustments of Na^+ and Cl^- concentrations, preserving electroneutrality.

Based on these assumptions, we write the following differential equations for L, the flux of hydrogen ions into the membrane, which then become either free intramembrane hydrogen ions or protons bound to pendant carboxyls, with respective concentrations C_{H} and C_{AH}, and the flux of H^+ to cell II:

$$\frac{dL}{dt} = -K_{\mathrm{w}}(1-\phi)\Bigg[\ln(1-\phi)+\phi+(\chi_1+\chi_2\phi)\phi^2+\nu_{\mathrm{w}}\rho_0\left(\frac{\phi_0}{\phi}-\frac{\phi}{2\phi_0}\right) - \nu_{\mathrm{w}}C_{\mathrm{NaCl}}\left(\lambda+\frac{1}{\lambda}-2\right)\Bigg], \tag{25}$$

$$\frac{d}{dt}[L(C_{\mathrm{H}}+C_{\mathrm{AH}})] = 2K_{\mathrm{h}}(1-\phi)\left[\lambda\frac{(C_{\mathrm{H}}^{\mathrm{I}}+C_{\mathrm{H}}^{\mathrm{II}})}{2}-C_{\mathrm{H}}\right], \tag{26}$$

$$\frac{d}{dt}C_{\mathrm{H}}^{\mathrm{II}} = \frac{AK_{\mathrm{G}}^{0}}{V}e^{-\beta\phi}C_{\mathrm{G}}-\frac{AK_{\mathrm{h}}}{V}(1-\phi)(\lambda C_{\mathrm{H}}^{\mathrm{II}}-C_{\mathrm{H}})-k_{\mathrm{mar}}C_{\mathrm{H}}^{\mathrm{II}}, \tag{27}$$

where V is the volume of Cell II and C_{G} is the glucose concentration in Cell I. Then, the governing system consists of (25)–(27) together with the algebraic constraints (1), (15), (18), and (21). With an additional scaling argument, we obtain the equations to analyze.

5. Model scaling and the governing system. In this section, we identify the relevant parameters of the system and their numerical values. This will allow us to rigorously derive a reduced model from the system (25)–(27). Five dimensionless groups give the system multiscale structure and properties, such as the role of the lower dimensional manifold discussed in section 7. However, the full dynamics cannot

be explained in terms of the dimensionless parameter groups only. We find that the range of the oscillatory behavior is further determined by a few individual parameters, such as C_{NaCl}, σ_0, and ϕ_0, with the remaining ones held fixed.

For convenience, we relabel the variable fields of the problem and define dimensionless variables:

$$x = C_{\mathrm{H}}, \quad y = C_{\mathrm{AH}}, \quad z = C_{\mathrm{H}}^{\mathrm{II}}, \quad h = C_{\mathrm{H}}^{\mathrm{I}}, \tag{28}$$

$$\bar{x} = \frac{x}{c}, \quad \bar{y} = \frac{y}{c}, \quad \bar{z} = \frac{z}{c}, \quad \bar{L} = \frac{L}{L_0}, \quad \bar{t} = \frac{t}{T}, \tag{29}$$

where T and c are typical time and concentration variables, respectively. For now, we use the superimposed *bar* notation to represent dimensionless quantities. We choose

$$T = \frac{L_0 \phi_0}{K_{\mathrm{w}}}, \quad c = K_{\mathrm{A}}. \tag{30}$$

Note that T corresponds to the time scale of (25), which will allow us to properly separate the dynamics of the membrane from that of the chemical reactions. The choice of c will lead to a reduced model resulting from the simplification of (26), as we shall see later in the section.

We now introduce five relevant dimensionless parameter groups consistent with the proposed scaling:

$$\mathcal{A}_1 = \frac{A}{V}\frac{C_{\mathrm{G}}}{K_{\mathrm{A}}}K_{\mathrm{G}}^0 T, \;\; \mathcal{A}_2 = \frac{A}{V}TK_{\mathrm{H}}, \;\; \mathcal{A}_3 = k_{\mathrm{mar}}T, \;\; \mathcal{A}_4 = 2\frac{K_{\mathrm{H}}}{K_w}\phi_0\frac{K_{\mathrm{A}}\phi_0}{\sigma_0}, \;\; \mathcal{A}_5 = \frac{K_{\mathrm{A}}\phi_0}{\sigma_0}. \tag{31}$$

5.1. Parameters of the model. These are shown in Tables (S2)–(S4) of the Supplementary Materials and are of three main types: device specifications, hydrogel parameters, and rate quantities. It should be noted that while some of these values either reflect the experimental conditions or are literature parameters for NIPA/MAA hydrogels [25], some parameters were chosen to produce results that are in line with experimental observations. Specifically, the size of the marble component in Cell II was chosen with a sufficiently large surface area so as to provide the necessary reaction sites to remove excessive hydrogen ions from the system.

DEFINITION 5.1. *We let $\mathcal{P}$ denote the set of parameters in Tables* (S2)–(S4) *of the Supplementary Materials and with*

$$C_{NaCl} \in [20 * 10^{-3}, 155 * 10^{-3}]M, \quad \sigma_0 = [0.10, 0.40], \quad \phi_0 = [0.1, 0.3]. \tag{32}$$

Experiments have been carried out with values of C_{NaCl} in the list $\{350, 250, 150, 100, 50, 40, 25, 20\} * 10^{-3}$M. However, for salt concentration values above $155 * 10^{-3}$M, no oscillatory behavior has been found. For parameter values in $\mathcal{P}$, we find typical magnitudes

$$\begin{gathered} \mathcal{A}_1 \approx 0.16 * 10^{1}, \quad \mathcal{A}_2 \approx 0.52 * 10^{-2}, \quad \mathcal{A}_3 \approx 0.75 * 10^{-2}, \\ \mathcal{A}_4 \approx 0.33 * 10^{-5}, \quad \mathcal{A}_1^0 := A_1 e^{-\beta\phi_0} = 0.016, \quad \mathcal{A}_5^{-1} \approx 3 * 10^{4}. \end{gathered} \tag{33}$$

The latter estimate combined with (15) allows us to write the scaled form of (18) as

$$\bar{y} = \mathcal{A}_5^{-1}\frac{\phi\bar{x}}{1+\bar{x}}, \;\; \text{so} \;\; \bar{x} + \bar{y} = \bar{x}\left(1 + \mathcal{A}_5^{-1}\frac{\phi}{1+\bar{x}}\right) = \mathcal{A}_5^{-1}\frac{\bar{x}\phi}{1+\bar{x}} + O(1). \tag{34}$$

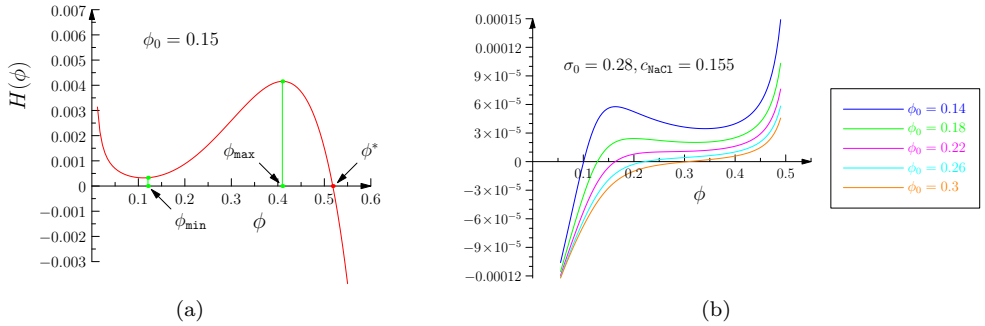

(a) (b)

FIG. 4. (a) *Plot of the mechanical compliance* $H(\phi)$ *for parameters values* $\chi_1 = .48, \chi_2 = .6$ *and* $\phi_0 = .3$, $\phi^* = 0.5226$. (b) *Plot of the left-hand side function of* (56).

We apply estimate (34) to simplify the scaled version of (26), which together with (25) and (27) gives the set of equations of the model that we analyze:

$$\frac{d\phi}{d\bar{t}} = \mathcal{R}_1, \tag{35}$$

$$\frac{d\bar{x}}{d\bar{t}} = \mathcal{A}_4\mathcal{R}_2 + \mathcal{A}_5(1+\bar{x})^2\mathcal{R}_1, \tag{36}$$

$$\frac{d\bar{z}}{d\bar{t}} = \mathcal{A}_1\mathcal{R}_3, \tag{37}$$

$$\lambda = p(\phi)f + \sqrt{p^2(\phi)f^2 + 1}, \quad f = (1+\bar{x})^{-1}, \tag{38}$$

where

$$\mathcal{R}_1(\phi,\lambda) = (1-\phi)\phi^2\big(H(\phi) - R(\lambda)\big), \quad \mathcal{R}_2(\phi,\bar{x},\lambda) = (1-\phi)(1+\bar{x})^2\left(\frac{\lambda}{2}\bar{z} - \bar{x}\right), \tag{39}$$

$$\mathcal{R}_3(\phi,\bar{x},\bar{z},\lambda) = e^{-\beta\phi} - \mathcal{A}_2\mathcal{A}_1^{-1}(1-\phi)(\lambda\bar{z} - \bar{x}) - \mathcal{A}_3\mathcal{A}_1^{-1}\bar{z}, \quad \text{and} \tag{40}$$

$$H(\phi) = \ln(1-\phi) + \phi + (\chi_1 + \phi\chi_2)\phi^2 + \bar{\nu_{\mathrm{w}}}\bar{\rho}_0\left(\frac{\phi_0}{\phi} - \frac{\phi}{2\phi_0}\right), \tag{41}$$

$$R(\lambda) = \nu_{\mathrm{w}}C_{\mathrm{NaCl}}\left(\sqrt{\lambda} - \frac{1}{\sqrt{\lambda}}\right)^2, \quad p(\phi) = \frac{\gamma\phi}{2(1-\phi)}, \tag{42}$$

$$q(\phi) = 1 + \frac{1}{2\gamma_0}H(\phi), \quad \gamma = \frac{\sigma_0}{C_{\mathrm{NaCl}}\phi_0}, \quad \gamma_0 = v_{\mathrm{w}}C_{\mathrm{NaCl}}. \tag{43}$$

The properties of the function $H(\phi)$, whose graph is shown in Figure 4, are summarized next.

LEMMA 5.2. *Suppose that the parameters in* (41) *belong to* $\mathcal{P}$. *Then the function* $H(\phi)$ *is nonmonotonic in* $(0,1)$ *and satisfies*

(44)
$$\lim_{\phi\to 0^+} H(\phi) = \infty, \quad H(\phi) = O\left(\frac{1}{\phi}\right) \quad \textit{and} \quad \lim_{\phi\to 1^-} H(\phi) = -\infty, \quad H(\phi) = O(\log(1-\phi)).$$

Moreover, there exists a unique $\phi^* \in (0,1)$ *such that* $H(\phi^*) = 0$. *Furthermore,* $H(\phi)$ *has a unique local maximum* ϕ_{max} *and a unique local minimum* ϕ_{min} *in* $(0,\phi^*)$, *as shown in Figure* 4.

From a different point of view, we observe that for parameter values as in (32) and (34),

$$\mathcal{A}_1\mathcal{R}_3 = \mathcal{A}_1^0 e^{-\beta(\phi-\phi_0)} + \cdots . \tag{45}$$

Relations (44) and (45) are used in obtaining the forthcoming estimates on the solutions, guaranteeing their validity in the convex function space, and also the set of initial data,

$$\mathcal{I} = \{\mathbf{x} = (\phi, x, z) : \phi \in (0,1), x \in (0,\infty), z \in (0,\infty)\}. \tag{46}$$

5.2. Time scales and a reduced model. There are two main goals in the investigation of the time scales of the problem. First of all, we need to guarantee that solutions with initial data in $\mathcal{I}$ remain there for all time of existence. This is carried out in this subsection by deriving estimates based on the multiple time scales structure of the model. The analysis also yields a reduced system whose role is essential in understanding the dynamics. The relative sizes of the dimensionless parameters $\mathcal{A}_i$, in particular the fact that $\mathcal{A}_4 \ll 1$ in (36), indicates that x is the slow field of the problem. Accordingly, we define the time scale associated with x as

$$\tau = \mathcal{A}_4\bar{t} = \frac{\mathcal{A}_4}{T}t, \quad \epsilon := \mathcal{A}_4, \quad \mu = \frac{\mathcal{A}_4}{\mathcal{A}_1}. \tag{47}$$

So, the original dimensionless time variable $\bar{t}$ corresponds to the *fast* dynamics, whereas τ gives the *slow* time that now we take as reference. Using both time scales to rewrite the governing system yields

$$\frac{d\phi}{d\bar{t}} = \mathcal{R}_1(\phi, \lambda), \tag{48}$$

$$\frac{d\bar{x}}{d\tau} = \mathcal{R}_2(\phi, \bar{x}, \lambda) + \frac{K_{\mathrm{A}}\phi_0}{\sigma_0\mathcal{A}_4}(1+\bar{x})^2\mathcal{R}_1, \tag{49}$$

$$\frac{d\bar{z}}{d\tau} = \frac{\mathcal{A}_1^0}{\mathcal{A}_4}\mathcal{R}_3^0(\phi, \bar{x}, \bar{z}, \lambda), \tag{50}$$

together with (38). Here, we have used expression (45) and the notation $\mathcal{R}_3^0 = e^{-\beta\phi_0}\mathcal{R}_3 = O(1)$. For our typical parameter values, $\mathcal{A}_4 = 0.33 * 10^{-5}$, $\frac{K_{\mathrm{A}}\phi_0}{\mathcal{A}_4\sigma_0} = 10$, and $\frac{\mathcal{A}_1^0}{\mathcal{A}_4} = 5 * 10^3$. (The latter magnitude indicates that the field z evolves with an intermediate time scale; however, associating it with τ does not affect the forthcoming analysis due to the independence of $\mathcal{R}_1$ on z.) This motivates identifying a reduced model consisting of (49)–(50) together with the algebraic equation $0 = \mathcal{R}_1(\phi, \lambda)$ and (38). We also point out that the scaling falls through when $\phi > 0$ is arbitrarily small, that is, for highly swollen regimes. This follows from estimating (35) for $\phi > 0$ small as well as the observation that $\lambda = O(1)$ and $R(\lambda) \approx 0$. Specifically, for given $\varepsilon > 0$, and for $\phi \in (0, \varepsilon)$,

$$p(\phi) = \gamma\phi + o(\varepsilon), \quad \lambda = 1 + o(\varepsilon), \quad R(\lambda) = o(\varepsilon), \quad H(\phi) = v_{\mathrm{w}}\rho_0\frac{\phi_0}{\phi} + o(\varepsilon). \tag{51}$$

This allows us to establish the following lemma.

LEMMA 5.3. *Suppose that the parameters of the governing system belong to $\mathcal{P}$. Let $\tilde{T} > 0$ be such that $\phi = \phi(t)$ and $\lambda = \lambda(t)$ satisfy (35) for $t \in [0, \tilde{T}]$. Then*

$$\frac{d\phi}{dt} = \frac{\nu_w\rho_0}{\mathcal{A}_4}O\left(\frac{1}{\phi}\right) \text{ as } \phi \to 0^+. \tag{52}$$

Estimates (51) guarantee ϕ will remain bounded away from 0 and 1.

PROPOSITION 5.4. *Suppose that the parameters of the governing system belong to $\mathcal{P}$. Solutions of* (35) *corresponding to initial data in $\mathcal{I}$ have the property that ϕ remains bounded away from $\phi = 0$ and $\phi = 1$ for all time. Moreover, there exist positive numbers t_m and t_M, depending on the initial data, such that $\phi(t_m) > 0$ and $\phi(t_M) > 0$ are minimum and maximum values of ϕ, respectively.*

Proof. Let us first recall that ϕ^* denotes the largest value of ϕ such that $H(\phi^*) = 0$. From the governing equation for ϕ, we see that for initial data $\phi_i \geq \phi^*$, $\frac{d\phi}{dt} < 0$. This proves the boundedness of the orbit away from $\phi = 1$. Let us consider an orbit with initial data $\phi_i \in (0, \epsilon)$ and such that $\frac{d\phi}{dt} < 0$ at some $t > 0$. Integrating the governing equation for ϕ while taking into account the estimates in (51) on its right-hand side function yields $\phi(t) = \phi_i O(e^{\frac{t}{v_w \rho_0 \phi_0}})$. This contradicts the assumption that $\frac{d\phi}{dt} < 0$ at some $t > 0$ and so proves the statement of the proposition. ∎

Remark 5.5. Proposition 5.4 states that the solution ϕ of the governing system remains in the interval $(0, 1)$ for all time of existence. However, due to the separation of time scales, only disconnected subintervals of $(0, 1)$ are admissible. This is the topic of the next section.

To establish boundedness of the x and z components of the solution, we first rewrite (37) as

$$\frac{dz}{dt} + w(t)z = g(t) \text{ with } w := \mathcal{A}_2(\lambda(1-\phi)+1), \quad g := \mathcal{A}_1 e^{-\beta\phi} + \mathcal{A}_2(1-\phi)x, \tag{53}$$

and integrate it to obtain the following lemma.

LEMMA 5.6. *Suppose that the parameters of the governing system belong to $\mathcal{P}$. Suppose that $z_0 > 0$, $x = x(t)$, $\phi = \phi(t)$, and $\lambda = \lambda(t)$ are prescribed, continuous functions with $t \in [0, \hat{T}]$, for some $\hat{T} > 0$. Then, the solution of* (37) *satisfies the equation*

$$z(t) = E^{-1}(t)\left(z_0 + \int_0^t E(s)g(s)\,ds\right),\ t \in [0, \hat{T}],\ z_0 = z(0),\ \text{and } E(t) := \exp\int_0^t w(s)\,ds. \tag{54}$$

This result immediately applies to showing that solutions of (36) remain bounded away from $x = 0$.

LEMMA 5.7. *Suppose that the parameters of the governing system belong to $\mathcal{P}$. Suppose that $\phi = \phi(t)$ and $z = z(t) > 0$ are prescribed continuous functions for $t \geq 0$, and such that $\phi(t)$ and $z(t)$ remain bounded away from $\phi = 0$ and $z = 0$, respectively. Then the solution $x = x(t)$ of* (36) *corresponding to initial data $x(0) > 0$ remains bounded away from $x = 0$ for all $t > 0$.*

Proof. We argue by contradiction and assume that for a prescribed arbitrarily small $\epsilon > 0$, there exists $t_1 = t_1(\epsilon) > 0$ such that $0 \leq x(t) \leq x(t_1) \leq \varepsilon$ for $t \geq t_1$. A simple calculation using (38) gives

$$\lambda(t_1) = p(\phi(t_1)) + \sqrt{p^2(\phi(t_1)) + 1} + O(\varepsilon). \tag{55}$$

Hence, $\mathcal{R}_2(t_1) \geq (1 - \phi(t_1))(1 + x(t_1))^2(\frac{\lambda(t_1)}{2} z(t_1) - \varepsilon)$. So, $\frac{dx}{dt}(t_1) > 0$ and bounded away from 0, and therefore, $x(t)$ cannot further decrease to 0. ∎

The previous results allow us to conclude global existence in time of bounded solutions.

PROPOSITION 5.8. *Suppose that the parameters of the governing system belong to* $\mathcal{P}$. *Let* $\{\phi = \phi(t),\, x = x(t),\, z = z(t)\}$, $t \in [0, T)$, *denote a solution of the system* (35)–(37) *and* (38) *corresponding to initial data in* $\mathcal{I}$, *and with* $T > 0$ *representing the maximal time of existence. Then* $\{\phi(t), x(t), z(t)\}$ *are bounded and* $T = \infty$. *Moreover, the lower bounds are strictly positive and the upper bound of* ϕ *is strictly less than* 1. *Furthermore,* $\mathcal{I}$ *is invariant under the flow of the governing system.*

From now on, we assume that all variables are scaled, suppress the superimposed *bar* in the equations, and represent the governing system (35)–(37) in the form $\dot{\mathbf{x}} = \boldsymbol{f}(\mathbf{x})$, $\mathbf{x} \in \mathcal{I}$, with the components of $\boldsymbol{f}$ given by the right-hand side functions of the system. It is easy to check that $\boldsymbol{f}$ is continuously differentiable in $\mathcal{I}$ (46).

In order to simplify notation, we will use t to denote (dimensionless) time and use τ only when emphasis on the slower evolution is needed.

In summary, we have presented the parameters of the model and the system to be analyzed. Through a dimensional analysis, we identified the time scales of the problem, from which a two-dimensional system in the slow dynamics emerges. For the purpose of ensuring global existence in time of solutions, with initial data in (46), and also to ensure that solutions remain in the physically meaningful regime, boundedness of such solutions has to be established.

6. Hopf bifurcation: A numerical study. In this section, we identify a maximal set $\mathcal{P}$ of parameters for which the system shows oscillatory behavior by numerically investigating the Hopf bifurcation structure of the model.

Steady state values of the variables x, z, and ϕ satisfy

$$x = \frac{\lambda}{2} z, \quad z = \mathcal{A}_1 e^{-\beta\phi} \left(\mathcal{A}_2 (1-\phi) \frac{\lambda}{2} + \mathcal{A}_3 \right)^{-1},$$

$$\frac{p}{\sqrt{q^2-1}} - 1 - \frac{\mathcal{A}_1}{2} \lambda e^{-\beta\phi} \left(\mathcal{A}_2 (1-\phi) \frac{\lambda}{2} + \mathcal{A}_3 \right)^{-1} = 0. \tag{56}$$

These are obtained by setting the right-hand sides of the governing equations equal to zero, and using relations (39), (42), and (43). Figure 4(b) shows plots of the function on the left-hand side of (56), with the corresponding unique root, which, after substitution into equations for x and z, yields their steady state values. The computational results summarized next are found to be in full agreement with those of laboratory experiments.

1. For $C_{\text{NaCl}} = 0.155$ M:

a. We found that for each $\phi_0 = 0.1, 0.15, 0.2, 0.295$, there is a unique physically relevant steady state, that is, with $\phi < \phi^*$. We point out that this result is valid for $\phi_0 \in [0.1, 0.3]$. This is justified by the implicit function theorem applied to the left-hand side function in (56) with respect to each root. In this proof, we also use the fact that the slope of the tangent line to the graph at the intersection with the ϕ-axis is nonhorizontal, as shown in Figure 4(b).

b. The diagrams in Figure 5 show the curves in the different parameter planes where a Hopf bifurcation occurs. For each set of parameter values in the region between the upper and lower curves, the system has a unique, unstable, steady state, with a pair of complex conjugate eigenvalues with positive real part, and a third negative eigenvalue. The real part of the complex conjugate pair becomes negative as the parameters cross the bifurcation curves, and so, the stationary state becomes stable. This indicates that the bifurcation that takes place as the parameters cross the curves from the outside to the interior of the region is supercritical.

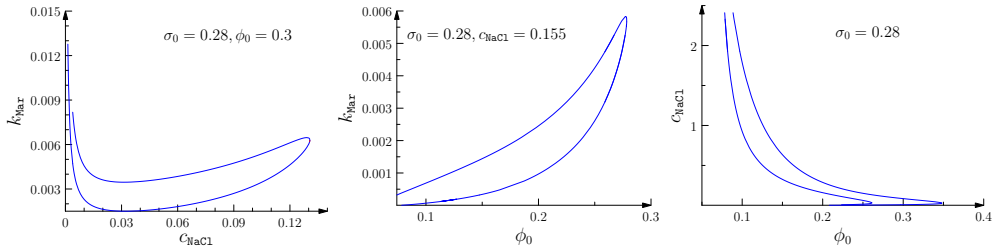

FIG. 5. *Hopf bifurcation diagrams in different parameter planes, computed with the software AUTO-07P.*

c. Oscillatory behavior is numerically found inside the regions determined by the curves in Figure 5.

2. We have also found that decreasing C_{NaCl} gives a qualitative behavior analogous to decreasing ϕ_0; that is, it promotes a single unstable stationary state of the system and the occurrence of Hopf bifurcation. This highlights the role of the marble in Cell II of the device (1). In particular, the following behaviors have been found:

a. For $C_{\mathrm{NaCl}} = 0.145$M and $\phi_0 = 0.3$, the steady state solution corresponds to $\phi = 0.145$.

b. For $C_{\mathrm{NaCl}} = 0.148$M and $\phi_0 = 0.3$, the maximum and minimum values of $x = x(s)$ occur at $\phi = 0.24$ and $\phi = 0.26$. In both these cases, a Hopf bifurcation has also been found.

c. Hopf bifurcations have also been found for $C_{\mathrm{NaCl}} = 0.125$M and $C_{\mathrm{NaCl}} = 0.115$M.

d. For $\phi_0 = 0.3$, $C_{\mathrm{NaCl}} = 0.155$M, and $\sigma_0 = 0.28$, no Hopf bifurcation occurs. The simulations do not show oscillatory behavior and there is at least one stable stationary state. Upon having identified a robust set of parameters for which the system has oscillatory behavior, we devote the next sections to analyzing its geometric and stability properties.

7. Inertial manifold of the governing system. We now derive and study a reduced two-dimensional system on a two-dimensional manifold $\mathcal{N}$ such that solutions of the initial value problem of the original three-dimensional system remain arbitrarily close to those of the reduced one for most of the time of existence. Moreover, we shall see that, for parameters in $\mathcal{P}$, the functions defining the two-dimensional system are specified in separate branches associated with the manifolds $\mathcal{M}$ and $\mathcal{M}^-$, the latter associated with the fast dynamics of the problem. Whereas $\mathcal{N}$ attracts solutions of the original system, $\mathcal{M}$ is the site of weak solutions, which encode the hysteresis and phase transition features of the model.

In order to identify the slow manifold, we consider the nullcline

$$H(\phi) = R(\lambda) \tag{57}$$

of the original system. This corresponds to setting $\epsilon = 0$ in (48), so that $\mathcal{R}_1 \equiv 0$ while keeping μ fixed.

We now list the properties of the solutions of (57) that follow from the positivity of $R(\lambda)$ and the fact that $\lambda \geq 1$.

LEMMA 7.1. *Let $H(\phi)$ and $R(\lambda)$ be as above. Then, solution pairs (ϕ, λ) of* (57)

satisfy

$$0 < \phi \le \phi^* \text{ so that } H(\phi) \ge 0 \quad \text{and} \quad \lambda > 1, \text{ with } \lambda = 1 \text{ when } \phi = \phi^*.$$

This allows us to characterize the nullcline (57) as

$$\begin{aligned} \mathcal{N} &= \{(\phi, \lambda, z) \in \mathbf{R}^3 : 0 < \phi < 1,\, z > 0, \lambda > 1, \\ H(\phi) &= R(\lambda), \text{ and such that (38) holds}\}, \end{aligned} \tag{58}$$

$$\mathcal{N} := \mathcal{N}^+ \cup \mathcal{N}^-,\ \ \mathcal{N}^+ = \{(\phi, \lambda, z) \in \mathcal{N} : H'(\phi) > 0\},$$

$$\mathcal{N}^- = \{(\phi, \lambda, z) \in \mathcal{N} : H'(\phi) \le 0\}. \tag{59}$$

Since relations (38) define λ as a monotonic function of x, we can exchange the roles of x and λ in (58)–(59) for convenience. Let us obtain an explicit representation of $\mathcal{N}$ and the governing equations of the reduced system. For this, we first solve (38) and (57) using (41), (42), and (43) as follows:

$$\frac{\gamma\phi}{(1-\phi)} f = \lambda - \frac{1}{\lambda}, \quad \frac{H(\phi)}{\gamma_0} = \lambda + \frac{1}{\lambda} - 2. \tag{60}$$

Addition and subtraction of these equations yield $\lambda = q(\phi) + p(\phi) f$ and $\frac{1}{\lambda} = q(\phi) - p(\phi) f$, respectively, which, in turn, give the equation $f_+ = \frac{1}{p}\sqrt{q^2 - 1}$ for $q \ge 1$ and with $H(\phi) \ge 0$. The corresponding values of the concentration x and the Donnan ratio λ are

$$x^+ = \frac{p(\phi)}{\sqrt{q^2(\phi) - 1}} - 1, \quad \lambda^+ = q(\phi) + \sqrt{q^2(\phi) - 1}, \tag{61}$$

respectively. Figure 6 presents the graphs of these functions, for parameters in the class $\mathcal{P}$, showing their nonmonotonicity as numerically verified. (Monotonicity of these curves has been found to hold outside the regions determined by the Hopf bifurcation curves in Figures 5, that is, outside the parameter space $\mathcal{P}$.) We label the critical points of $x^+(\phi)$ as

$$0 < \phi_s^1 < \phi_s^2 : \ \frac{dx^+}{d\phi}(\phi_s^i) = 0,\ i = 1, 2, \quad \text{and} \quad x_s^i := x^+(\phi_s^i), \tag{62}$$

and note that the strictly increasing branches correspond to the interval $(0, \phi_s^1) \cup (\phi_s^2, \phi^*)$. Let $\phi^+(x)$ represent the inverse of $x^+(\phi)$ defined in $(0, x_s^1) \cup (x_s^2, x^*)$. (Decreasing branches are associated with the intervals (ϕ_s^1, ϕ_s^2) and (x_s^1, x_s^2), respectively.) Let us define

$$\begin{aligned} \mathcal{M}_1 &:= \{(\phi, x, z) : z \ge 0,\, x = x^+(\phi),\, \phi \in (0, \phi_s^1)\}, \\ \mathcal{M}_2 &:= \{(\phi, x, z) : z \ge 0,\, x = x^+(\phi),\, \phi \in (\phi_s^2,\, \phi^*)\}, \\ \mathcal{M} &:= \mathcal{M}_1 \cup \mathcal{M}_2, \quad \mathcal{M}^- := \{(\phi, x, z) : z \ge 0,\, x = x^+(\phi),\, \phi \in (\phi_s^1,\, \phi_s^2)\}. \end{aligned} \tag{63}$$

The graph $x^+(\phi)$ represents the cross section with respect to z of the surface $H(\phi) = R(\lambda)$ which divides the whole space into upper and lower regions, with $\mathcal{R}_1 > 0$ and $\mathcal{R}_1 < 0$, respectively.

PROPOSITION 7.2. *Suppose that the parameters of the problem belong to the class $\mathcal{P}$. Then $\mathcal{N} = \mathcal{M} \cup \mathcal{M}^-$ is a two-dimensional invariant manifold of the three-dimensional system. Furthermore, the vector field of the two-dimensional system is Lipschitz in $\mathcal{M}$. Moreover, $\mathcal{N}^- \subset \mathcal{M}$.*

Proof. Let us consider initial data $(\phi_0, x_0, z_0) \in \mathcal{N}$. Since $H(\phi) = R(\lambda)$ is a nullcline of the system, we can construct a solution of the three-dimensional problem belonging to $\mathcal{N}$. So, by uniqueness, solutions with initial data satisfying $x_0 = x^+(\phi_0)$, $\phi_0 \in (0, \phi^*)$ belong to $\mathcal{N}$ for all time of existence. Moreover, applying the same arguments as in Proposition 5.8, we find that $x(t)$ remains bounded away from $x = 0$, and so $\phi(t) > \phi^{**}$ for all $t > 0$. The last statement of the proposition follows by taking the derivative with respect to ϕ of the function $x = x^+(\phi)$ in (61) to give

$$\frac{dx}{d\phi} = \frac{1}{\sqrt{q^2-1}}\left((1-\phi)^{-2} - \frac{pq}{q^2-1}H'(\phi)\right). \tag{64}$$

So, $H'(\phi) < 0$ implies that $\frac{dx}{d\phi} > 0$ for $\phi < \phi^*$. ∎

The governing system restricted to $\mathcal{M}$ reduces to (61) together with equations

$$\frac{dx}{dt} = \mathcal{A}_4\phi(1-\phi)(1+\gamma\phi f^2)^{-1}\left(\frac{\lambda}{2}z - x\right), \tag{65}$$

$$\frac{dz}{dt} = \mathcal{A}_1 e^{-\beta\phi} - \mathcal{A}_2(1-\phi)(\lambda z - x) - \mathcal{A}_3 z. \tag{66}$$

It is easy to see that the sets $\mathcal{M}_1$, $\mathcal{M}_2$, and $\mathcal{M}^{-1}$ are invariant manifolds of the two-dimensional system. However, the physically relevant solutions are the weak solutions, as characterized next, associated with the hysteresis loops in Figure 4(a).

Definition 7.3. *A weak solution of the two-dimensional system corresponding to initial data $(\phi^0, x^0, z^0) \in \mathcal{M}$ has the following properties:*

1. *There exists $0 < \hat{t}$ such that $(\phi(t), x(t), z(t))$ is a classical solution for $t \in (0, \hat{t})$.*
2. *$\phi(\hat{t}) = \phi_s^1$ (or ϕ_s^2).*
3. *$\phi(t)$ is discontinuous at $\hat{t}$ experiencing a jump $[\phi(\hat{t})] = \phi_s^2 - \phi_s^1$ (alternatively, $[\phi(\hat{t})] = \phi_s^1 - \phi_s^2$).*
4. *The time derivatives of ϕ experience finite time blow-up, that is, $\lim_{t\to\hat{t}} \frac{d\phi}{dt}(t) = +\infty$ (alternatively, $\lim_{t\to\hat{t}} \frac{d\phi}{dt}(t) = -\infty$).*
5. *$x(t)$ and $z(t)$ are continuous at $\hat{t}$ and their derivatives experience a jump discontinuity.*
6. *The solutions can be continued for $t > \hat{t}$ and are bounded.*

Remark 7.4. $\mathcal{M}$ is, by construction, invariant to weak solutions; $\mathcal{M}^-$, which is also an invariant manifold of the two-dimensional system, contains the unique stationary point, with eigenvalues forming a complex conjugate pair, with positive real part. The limit cycle of the two-dimensional system discussed at the end of this section is also the ω-limit set of solutions with initial data in $\mathcal{M}^-$. We point out that values of $\phi \in (\phi_s^1, \phi_s^2)$ are excluded from the range of weak solutions of the two-dimensional system, with ϕ experiencing jump discontinuities so as to avoid this interval. However, this interval is accessible to solutions of the full system, and, in particular, it contains the unique unstable equilibrium point. We will also show that this interval is covered in the fast time scale.

One main ingredient in the construction of weak solutions is the theorem on continuation and finite time blow-up of solutions of ordinary differential equations together with the existence of a unique, unstable, equilibrium point. This, together with the Poincaré–Bendixon theorem for two-dimensional systems, leads to the existence of a limit cycle for such a system. The latter is also the ω-limit set of the positive semiorbits of the three-dimensional system.

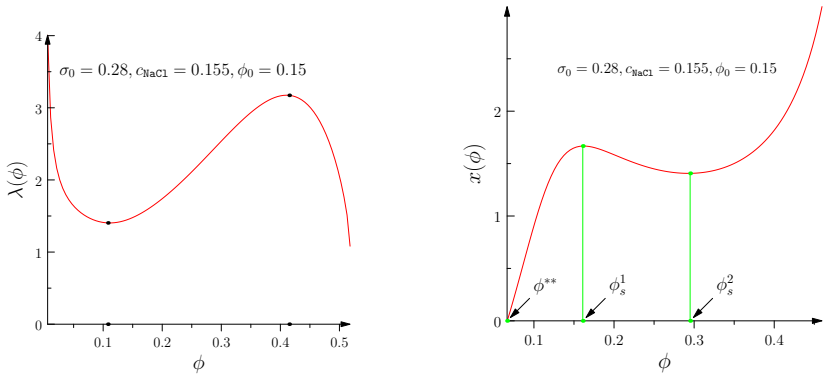

FIG. 6. *Plots of $\lambda = \lambda^+(\phi)$ and $x = x^+(\phi)$ in (61) representing cross sections of the slow manifold with respect to z.*

The following result follows from the uniqueness of classical solutions of the initial value problem of the system (35)–(42).

We denote the weak solution as $\boldsymbol{\psi}_{\mathcal{M},t} = (\phi_{\mathcal{M}}, x_{\mathcal{M}}(\phi), z_{\mathcal{M}})$, where $\boldsymbol{\psi}_{\mathcal{M},t}$ is the flow. Let $\boldsymbol{\varphi}_t$ denote the flow of the three-dimensional system with initial data in $\mathcal{I}$. In order to study solutions with initial data outside $\mathcal{M} \cup \mathcal{M}^-$, we observe the following properties of the term $\mathcal{R}_1$:

$$\mathcal{R}_1 > 0 \quad \text{for} \quad x > x^+(\phi) \quad \text{and} \quad \mathcal{R}_1 < 0 \quad \text{for} \quad x < x^+(\phi). \tag{67}$$

PROPOSITION 7.5. *Suppose that the parameters of the system belong to the class $\mathcal{P}$. Then the following statements on the three-dimensional system hold:*

1. *Solutions with initial data such that $x^0 \neq x^+(\phi^0)$ have the property that $|\mathcal{R}_1(\phi(t), x(t))|$ decreases with respect to t for sufficiently large $t > 0$. In particular, $|\mathcal{R}_1|$ is strictly decreasing for $\phi^0 \in (0, \phi_s^1) \cup (\phi_s^2, \phi^*)$ for all $t > 0$.*

2. *Let $\epsilon > 0$ be sufficiently small. Then $\mathcal{N}^-$ is asymptotically stable, that is, for sufficiently large t, solutions corresponding to initial data $(\phi^0, x^0, z^0) \in \mathcal{I}$ satisfy*

$$\phi(t) = \Phi(\tau) + O(e^{-\frac{\tau}{\epsilon}}), \quad x(t) = X(\tau) + O(e^{-\frac{\tau}{\epsilon}}), \quad z(t) = Z(\tau) + O(e^{-\frac{\tau}{\epsilon}}), \quad t = \frac{\tau}{\epsilon}, \tag{68}$$

where $(\Phi(\tau), X(\tau), Z(\tau)) \in \mathcal{N}^-$ is the solution of the two-dimensional system corresponding to initial data $(\phi_0, x^+(\phi_0), z_0)$.

Proof. Part 1 follows directly from the first equation in (39), the properties of the functions $H(\phi)$ and $R(\lambda)$, and (35). Due to the time scale structure of the system, it is sufficient to prove the first of the relations (68). Let us write $\phi(t) = \Phi(\tau) + \tilde{\phi}(t)$ and linearize $\mathcal{R}_1$ in (39) about (Φ, Λ) to obtain

$$\frac{d\tilde{\phi}}{dt} = -M(\phi_0, \lambda^+(\phi_0))\tilde{\phi}(t) + o(\tilde{\phi}, \epsilon), \quad M(\Phi, \Lambda) := \frac{\partial \mathcal{R}_1}{\partial \phi}(\Phi, \Lambda) + \frac{\partial \mathcal{R}_1}{\partial \lambda}(\Phi, \Lambda)\frac{\partial \lambda}{\partial \phi}. \tag{69}$$

An explicit calculation gives

$$M(\Phi, \Lambda) = -\frac{1}{2}(1 - \Phi)\Phi^2 \left(H'(\Phi)\left(1 + \frac{1}{\Lambda^2}\right) - \frac{\gamma\gamma_0}{2(1 - \Phi^2)} f(X)\left(1 - \frac{1}{\Lambda^2}\right)\right). \tag{70}$$

Note that the exponential decay follows immediately for $(\phi_0, x_0, z_0) \in \mathcal{N}^- \subset \mathcal{M}$, where $M > 0$. Otherwise, we appeal to (49), Proposition 5.8, existence of a unique (unstable) equilibrium point, and property (67) to find a finite time $t_1 > 0$ such that $H'(\phi(t_1)) < 0$, reducing the problem to the prior case. ∎

Remark 7.6. Note that the first inequality may still hold in the case that $H'(\phi^0) > 0$, that is, for $\phi_0 > \phi_{\min}$ or $\phi_0 < \phi_{\max}$ in Figure 4. This property is referred to as the reduced system having a *canàrd* structure [4, 27]. The case $M = 0$ cannot be characterized in terms of linear stability.

The next theorem characterizes the long time behavior of solutions of both systems.

THEOREM 7.7. *For each set of initial data $(\phi^0, x^0, z^0) \in \mathcal{M}$, there is a unique weak solution $(\phi_{\mathcal{M}}, x_{\mathcal{M}}, z_{\mathcal{M}}) \in \mathcal{M}$ of the two-dimensional system that exists for all $t > 0$. Moreover, the ω-limit set $\omega(\pi^+)$ of a semiorbit π^+ of the three-dimensional system with initial data in $\mathcal{I}$ satisfies $\omega(\pi^+) = \omega(\pi^+_{\mathcal{M}})$, where $\omega(\pi^+_{\mathcal{M}})$ is the ω-limit set of the trajectories of the two-dimensional system.*

Proof. Without loss of generality let us assume that $(\phi(0), x(0), z(0)) \in \mathcal{M}_2$ and with $\frac{1}{2}\lambda(x(0), \phi(0))z(0) - x(0) < 0$. Then, there is $\hat{t} > 0$ such that $(0, \hat{t})$ gives the maximal interval of existence of the classical solution of the two-dimensional system. Two different situations may occur, according to the choice of initial data:

1. $\hat{t} = \infty$, in which case the solution is bounded and such that $x(t) \in \mathcal{M}_2$ for all time, or
2. $0 < \hat{t} < \infty$, in which case $x(\hat{t}) = x^2_s$ and $\phi(\hat{t}) = \phi^2_s$.

In case 2, we further distinguish two cases, also according to initial data:

2a. $\frac{1}{2}\lambda(x(\hat{t}), \phi(\hat{t}))z(t) - x(\hat{t}) = 0$, in which case $\frac{dx}{dt}(\hat{t}) = 0$. The solution can then be continued as in case 1, that is, as a classical solution in $\mathcal{M}_2$, and so it never reaches $\mathcal{M}_1$.

2b. $\frac{1}{2}\lambda(x(\hat{t}), \phi(\hat{t}))z(\hat{t}) - x(\hat{t}) < 0$, and so $\frac{dx}{dt}(\hat{t}) < 0$. Since $\lim_{t\to\hat{t}} \frac{dx}{d\phi}(t) = 0$, then $\lim_{t\to\hat{t}} \frac{d\phi}{dt}(t) = -\infty$. We set $\phi(\hat{t}^+) = \phi^1_s$, so the jump condition $[\phi] = \phi^1_s - \phi^2_s$ is satisfied, $x(\hat{t}^-) = x(\hat{t}^+) = x^2_s$, and $z(\hat{t}^-) = z(\hat{t}^+)$. Note that at $t = \hat{t}^+$, $(\phi, x, z) \in \mathcal{M}_1$.

To continue the solution for $t > \hat{t}$, we solve the initial value problem with initial data $(\phi(\hat{t}^+), x(\hat{t}^+), z(\hat{t}^+))$. It is easy to see that there is a time $\tilde{t} > \hat{t}$ such that $\lim_{t\to\tilde{t}^-} \phi(t) = \phi^1_s$ and $\lim_{t\to\tilde{t}^-} x(t) = x^1_s$. In fact, this follows from the fact that ϕ and x remain bounded away from 0, so that the values ϕ^1_s and x^1_s, respectively, can be reached, allowing the solution to be continued in $\mathcal{M}_2$. The fact that $\phi < \phi^*$ and that there are no equilibrium points in $\mathcal{M}_2$ guarantees the existence of a point of return on the trajectory $(\phi(t), x(t), z(t))$, and so the process can be continued.

Since the orbits π^+ and $\pi^+_{\mathcal{M}}$ are both bounded, the scaling with respect to $\mathcal{A}_4$ holds, and so does the estimate

$$|\phi(t) - \phi_{\mathcal{M}}(\tau)| = O(e^{-t}), \tag{71}$$

together with the analogous estimates for $x(t), z(t)$, which completes the proof of the theorem. ∎

Note that $\omega(\pi_{\mathcal{M}^-}{}^+) = \omega(\pi^+_{\mathcal{M}})$ also holds as a result of the instability of the equilibrium point.

Remark 7.8. The orbits of the two-dimensional system analyzed in this section, and in particular the limit cycle, correspond to the projection to the $x - z$ plane of the three-dimensional orbits shown in Figure 7(b).

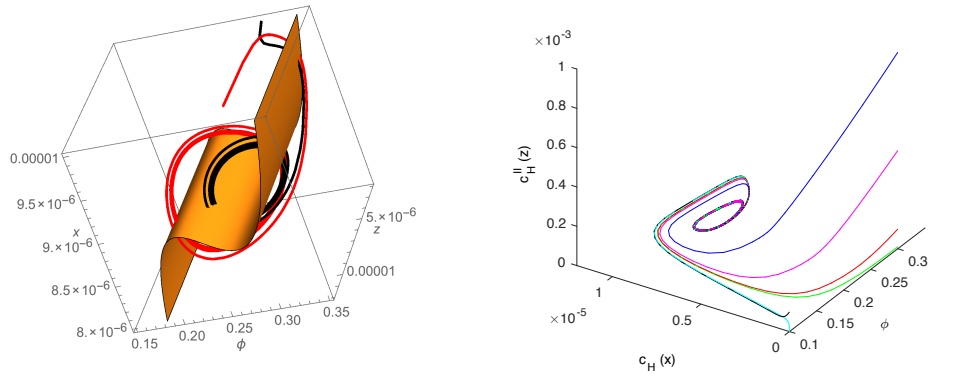

(a) (b)

FIG. 7. *Figure* (a) *shows orbits of the three-dimensional system and the manifold* $\mathcal{M}$. *Figure* (b) *shows plots of orbits of the three-dimensional system approaching a plane closed curve. It is the* ω*-limit set of both systems and the limit cycle of the two-dimensional system in the manifold* $\mathcal{N}$.

Since $\mathcal{M}$ is an invariant set that does not contain equilibrium points, the existence of a limit cycle for the two-dimensional system follows from the Poincaré–Bendixon theorem. Its corollary gives the stability of the limit cycle with respect to both the two-dimensional and three-dimensional dynamics [15]. The next theorem shows that the limit cycle of the two-dimensional system is also the limit cycle of the three-dimensional one.

THEOREM 7.9. *Suppose that the parameters of the system belong to the class* $\mathcal{P}$. *Then the two-dimensional system has an asymptotically stable limit cycle* π^+ *in* $\mathcal{M}$. *Moreover,* π^+ *is also the* ω*-limit set of positive semiorbits of the three-dimensional system with initial data in* $\mathcal{I}$.

Proof. Let us consider solutions with initial data in $\mathcal{M}$. For these initial data, we previously showed that the two-dimensional system admits bounded weak solutions that exist for all time. Moreover, the orbits of these solutions do not contain any equilibrium point. So, the existence of a limit cycle π^+ in $\mathcal{M}$ follows directly from the Poincarè–Bendixon theorem. The asymptotic stability of π^+ follows from the boundedness of solutions and the absence of a stationary state in $\mathcal{M}$. To prove the last statement, let us consider solutions with initial data $(\phi^0, x^0, z^0) \in \mathcal{I}$ and such that $x^0 \neq x^+(\phi^0)$. By an estimate as (71), we can assert that for sufficiently large t, $|x(t) - x_M(t)| = O(e^{-Mt})$, with $M > 0$ as in (69), and $x_M(t) := x_M(\phi^0, x^+(\phi^0), z^0)(t)$. This indicates that the solution of the three-dimensional system approaches the two-dimensional manifold for sufficiently large t. Since the only equilibrium point in the three-dimensional space is unstable, the three-dimensional solution also approaches the limit cycle (Figure 7(b)). ∎

Remark 7.10. We observe that the solutions of the plane system, and in particular the limit cycle, are discontinuous with respect to ϕ. In particular, ϕ is discontinuous at $t = \hat{t}$, with $[\phi(\hat{t})] \neq 0$. The regularization of the solutions is done by *connecting* the discontinuity values of ϕ by a function $\bar{\phi}(\frac{t}{\mathcal{A}_4})$ that evolves according to the *fast* dynamics presented in the next section. For sufficiently small $\mathcal{A}_4$, the solutions of the three-dimensional system remain in $\mathcal{M}$ for most of the time, emerging to the third

dimension in order to connect the separate branches $\mathcal{M}_1$ and $\mathcal{M}_2$ in the fast time scale.

We have found that the limit cycle of the two-dimensional system is also the ω-limit set of solutions of the full system. In the next section, we will further establish it as the limit cycle of the three-dimensional system.

8. Competitive systems and three-dimensional limit cycle. It is well known that for three-dimensional systems, the compactness of a steady state free ω-limit set of an orbit is not sufficient to prove the existence of a periodic orbit. That is, the Poincaré–Bendixon theorem in its original form does not apply. However, a three-dimensional generalization is available for *competitive* (and *cooperative*) systems (see [17, 18, 19, 31]). This concept is framed in terms of monotonicity properties of the vector field $\mathbf{f} = (f_1, f_2, f_3)$ of the system $\dot{\mathbf{x}} = \mathbf{f}(\mathbf{x})$, with respect to a convex subspace of $\mathbb{R}^3$. The theorem is due to Hirsch, and it is stated as follows.

THEOREM 8.1. *A compact limit set of a competitive or cooperative system in* $\mathbf{R}^3$ *that contains no equilibrium points is a periodic orbit.*

A dynamical system is called *competitive* in the positive cone $\mathbb{R}^{+n}$ if $\frac{\partial f_i}{\partial x_j}(\mathbf{x}) \leq 0,\ i \neq j,\ \mathbf{x} \in \mathcal{I}$. This property holds in a general cone $\mathcal{K}$ (intersection of half-spaces) by requiring the following two properties.

DEFINITION 8.2. *A* $n \times n$ *Jacobian matrix* $(\nabla \boldsymbol{f})$ *is sign-stable in* $\mathcal{I}$ *if for each* $i \neq j$, *either* $\frac{\partial f_i}{\partial x_j} \geq 0$ *or* $\frac{\partial f_i}{\partial x_j} \leq 0$ *for all* $\mathbf{x} \in \mathcal{I}$. *It is sign-symmetric if* $\frac{\partial f_i}{\partial x_j}(\mathbf{x})\frac{\partial f_j}{\partial x_i}(\mathbf{y}) \geq 0$ *for all* $i \neq j$ *and for all* $\mathbf{x}, \mathbf{y} \in \mathcal{I}$.

PROPOSITION 8.3. *The three-dimensional governing system* (35)–(38) *is competitive with respect to the cone* $\mathcal{K} = \{(\phi, x, z) : \phi < 0,\ x > 0,\ z < 0\}$.

The proof involves identifying $\mathcal{K}$ and verifying definition (8.2), which follows from these two lemmas.

LEMMA 8.4. *The inequalities* $\phi(1-\phi)\frac{\partial \lambda}{\partial \phi} = \lambda \frac{fp}{\sqrt{1+p^2 f^2}} \geq \lambda$ *and* $\frac{\partial \lambda}{\partial x} < 0$ *hold on trajectories* $\boldsymbol{\varphi}_t$ *corresponding to initial data in* $\mathcal{I}$.

Proof. For λ, p, and f as in (38) and (43), simple calculations show that

$$\frac{2}{\gamma}(1-\phi)^2\frac{\partial \lambda}{\partial \phi} = \frac{f}{\sqrt{1+p^2f^2}} = \frac{f\lambda}{\sqrt{1+p^2f^2}} = \frac{2}{\gamma}\frac{(1-\phi)}{\phi}\frac{fp\lambda}{\sqrt{1+p^2f^2}},$$

$$\frac{\partial \lambda}{\partial x} = \frac{pf'}{\sqrt{1+p^2f^2}}\lambda = -\frac{p}{(1+x)^2}\frac{\lambda}{\sqrt{1+p^2f^2}} > -\frac{p}{(1+x)^2}\lambda, \tag{72}$$

from which the stated inequalities follow. ∎

LEMMA 8.5. *The Jacobian matrix* $\mathcal{J}$ *of the three-dimensional system is sign-stable and sign-symmetric.*

Proof. Let us calculate the Jacobian matrix $J := \{a_{ij}\}$ at an arbitrary state (ϕ, x, z):

$$a_{12} = -(1-\phi)\phi^2 R'(\lambda)\frac{\partial \lambda}{\partial x}, \quad a_{21} = (1-\phi)(1+x)^2\frac{z}{2}\frac{\partial \lambda}{\partial \phi} - (1+x)^2\left(\frac{\lambda}{2}z - x\right), \tag{73}$$

$$a_{31} = -\beta e^{-\beta\phi} - \frac{\mathcal{A}_2}{\mathcal{A}_1}\left((1-\phi)z\frac{\partial \lambda}{\partial \phi} - (\lambda z - x)\right), \quad a_{13} = 0, \tag{74}$$

$$a_{23} = (1-\phi)(1+x)^2\frac{\lambda}{2}, \quad a_{32} = -\frac{\mathcal{A}_2}{\mathcal{A}_1}(1-\phi)\left(z\frac{\partial \lambda}{\partial x} - 1\right). \tag{75}$$

Note that the off-diagonal elements of the matrix J have the following signs:

$$a_{12} > 0, \quad a_{13} = 0, \quad a_{23} > 0, \quad a_{32} > 0, \quad a_{21} > 0, \quad a_{31} < 0,$$

from which sign-symmetry and sign-stability immediately follow. For this, let us write

$$a_{21} = (1+x)^2\left((1-\phi)\frac{\partial\lambda}{\partial\phi}\frac{z}{2} - \frac{\lambda}{2}z + x\right) > \frac{x}{(1+x)^2} > 0. \tag{76}$$

Note that $a_{23} > 0$ and $a_{31} < -\beta e^{-\beta\phi} - \frac{\mathcal{A}_2}{\mathcal{A}_1}x < 0$, where we have used the first inequality in Lemma 8.4. Finally, to check the sign of a_{12}, we differentiate $R(\lambda)$ in (42) to find $R'(\lambda) = (\sqrt{\lambda} - \frac{1}{\sqrt{\lambda}})(\lambda^{-\frac{1}{2}} + \lambda^{-\frac{3}{2}})$, from which the sign of a_{12} follows, taking into account the second inequality in Lemma 8.4. The identification of the corresponding cone $\mathcal{K}$ is done in the Supplementary Materials. ∎

One of the practical difficulties in the application of the Poincaré–Bendixon theorem to three-dimensional systems as compared to the two-dimensional counterpart is the verification that the ω-limit set does not contain equilibrium points. The case that the system has a single unstable equilibrium point is the simplest one to treat. Existence of a three-dimensional limit cycle, together with additional properties of competitive systems relevant to the current analysis, is summarized next.

THEOREM 8.6. *Let $\mathcal{P}$, $\mathcal{M}$, and $\mathcal{I}$ be as in Definitions* 5.1, (46), *and* (63), *respectively. Then we have the following:*

1. *The flow on the ω-limit set of orbits of the three-dimensional system in $\mathcal{I}$ is topologically equivalent to the flow on the ω-limit set of orbits of the two-dimensional system in $\mathcal{M}$.*
2. *Let $\mathbf{p} = (\Phi, X, Z)$ be the unique equilibrium point of the system. If $\mathbf{p} \neq \mathbf{q} \in \mathcal{I}$, then $\mathbf{p} \notin \omega(\mathbf{q})$.*
3. *The three-dimensional system has a limit cycle.*

Proof. The first item follows from the fact that the two-dimensional system is Lipschitz, the competitiveness of the three-dimensional system, and the compactness of the ω-limit set of both systems. The second statement follows from competitiveness and the fact that the equilibrium point is unique and hyperbolic. In fact, it is a consequence of the theorem that *a compact limit set of a competitive or cooperative system cannot contain two points related by* $\ll$ (see [31, Theorem 3.2]). Finally, property 3 is a consequence of 2, the compactness of the ω-limit set, and Theorem 8.1. Plots of the solutions of the three-dimensional system are shown in Figure 8. ∎

Remark 8.7. In the case that the unique equilibrium point $\mathbf{p}$ is hyperbolic, to prove that $\mathbf{p} \notin \omega(\mathbf{q})$, $\mathbf{q} \in \mathcal{D}$, it is necessary to assume that the system is competitive. This is the case encountered in some applications such as in virus dynamics [23].

Remark 8.8. We consider the model obtained by further reducing the time scale, that is, setting the limiting problem in the *slow* scale as $0 = \mathcal{R}_1(\phi, \lambda)$, $\frac{d\bar{x}}{d\tau} = \mathcal{R}_2(\phi, \bar{x}, \lambda)$, $0 = \mathcal{R}_3(\phi, \bar{x}, \bar{z}, \lambda)$, together with (38). This is consistent with taking $\frac{\mathcal{A}_4}{\mathcal{A}_1} = O(\epsilon^{-3})$. This model yields that which was proposed by Li and Siegel [24], which sets a relay equation for the *product* of the reaction, in this case, the hydrogen ion concentration in the membrane.

9. Concluding remarks. The model presented here dealt with the fundamental mechanisms underlying oscillatory behavior of a table-top experimental device. It must be regarded as a first step towards developing an in-vivo device, due to chemical

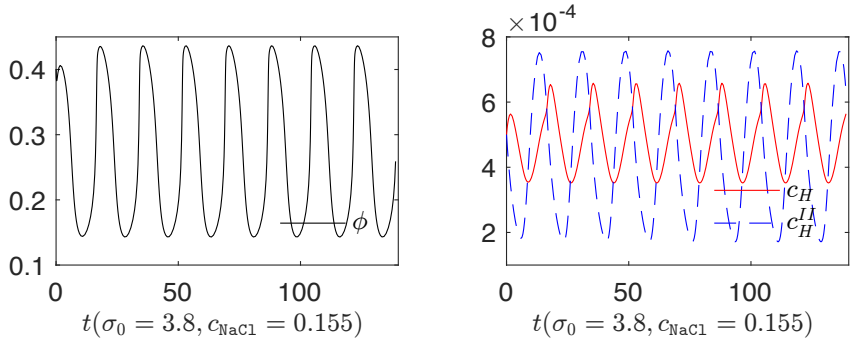

FIG. 8. *The left plot represents the swelling dynamics of the membrane in terms of the polymer volume fraction. The graphs of the right plot refer to the evolution of H^+ in the membrane (red) and in Cell II (blue), respectively. The oscillatory behavior is compatible with the GnRH pulse release. (Figure appears in color online.)*

and mechanical hurdles that still need to be overcome. First of all, there are complications associated with the buildup of gluconate ion in the system, which buffers and affects the dynamics of pH oscillations, and has not been included in the present model. Also, the effects of endogenous phosphate and bicarbonate buffering species would need to be included in a more comprehensive model, which would be of higher dimensionality, even in the lumped framework. Second, design changes in the device would have to be made to overcome the effect of the signature gel undulation instability in gel free surfaces, which tends to counter the oscillatory pattern. In particular, this would require formulating the problem as a system of partial differential equations that, in addition to more accurately portraying the physical situation, would accommodate the proper boundary conditions at the interfaces between the membrane and the two chambers. The main results presented here are not expected to be altered qualitatively, though there will be quantitative differences. Although the device presented here is unique and original, the general laws that govern its functioning are widely applicable to the design of microfluidic devices such as rhythmically operating valves in materials sciences and biological settings. To the best of our knowledge, rhythmic gel devices driven by temperature gradient have not yet been developed. However, a great deal of effort is being devoted to the design of microfluidic liquid crystal elastomer devices, for instance, in the form of temperature activated valves and electric field driven devices [21]. New technologies in particle transport are also being developed in colloidal based liquid crystals [22], where the topology plays a main role in driving and controlling particle flow. A great deal of effort is also currently being devoted to energy transformation devices based on phase transitions in crystalline materials [32].

REFERENCES

[1] A. A. ADRONOV, A. A. VITT, AND S. E. KHAIKHIN, *Theory of Oscillators*, International Series of Monographs in Physics 4, Pergamon Press, Oxford, 1966.

[2] J. P. BAKER AND R. A. SIEGEL, *Hysteresis in the glucose permeability versus ph characteristic for a responsive hydrogel membrane*, Macromol. Rapid. Commun., 17 (1996), pp. 409–415, https://doi.org/10.1002/marc.1996.030170607.

[3] A. S. Bhalla and R. A. Siegel, *Mechanistic studies of an autonomously pulsing hydrogel-enzyme system for rhythmic hormone delivery*, J. Control. Release, 196 (2014), pp. 261–271, https://doi.org/10.1016/j.jconrel.2014.10.019.
[4] K. Bold, C. Edwards, J. Guckenheimer, S. Guharay, K. Hoffman, J. Hubbard, R. Oliva, and W. Weckesser, *The forced van der Pol equation* II: *Canards in the reduced system*, SIAM J. Dyn. Syst., 2 (2003), pp. 570–608, https://doi.org/10.1137/S1111111102419130.
[5] A. P. Dhanarajan, *Mechanistic Studies and Development of a Hydrogel-Enzyme Drug Delivery Oscillator*, Ph.D. thesis, University of Minnesota, Minneapolis, MN, 2004.
[6] A. P. Dhanarajan, G. P. Misra, and R. A. Siegel, *Autonomous chemomechanical oscillations in a hydrogel-enzyme system driven by glucose*, J. Phys. Chem. A, 106 (2002), pp. 8835–8838, https://doi.org/10.1021/jp026086v.
[7] A. English, T. Tanaka, and E. Edelman, *Polyelectrolyte hydrogel instabilities in ionic solutions*, J. Chem. Phys., 105 (1996), pp. 10606–10613, https://doi.org/10.1063/1.472946.
[8] I. Epstein and J. Pojman, *An Introduction to Nonlinear Chemical Dynamics*, Oxford University Press, New York, 1998.
[9] B. Erman and P. Flory, *Critical phenomena and transitions in swollen polymer networks in and linear macromolecules*, Macromolecules, 19 (1986), pp. 2342–2353, https://doi.org/10.1021/ma00163a003.
[10] B. A. Firestone and R. A. Siegel, *Dynamic pH-dependent swelling properties of a hydrophobic polyelectrolyte gel*, Polymer Communications, 29 (1988), pp. 204–208.
[11] P. Flory, *Principles of Polymer Chemistry*, Cornell University, Ithaca, NY, 1953.
[12] A. Goldbeter, *Biochemical Oscillations and Cellular Rhythms*, Cambridge University Press, Cambridge, UK, 1996.
[13] P. Gray and S. Scott, *Chemical Oscillations and Instabilities*, International Series of Monographs on Chemistry 21, Oxford University Press, Clarendon, Oxford, UK, 1990.
[14] P. Grimshaw, J. Nussbaum, A. Grodzinsky, and M. Yarmush, *Kinetics of electrically and chemically induced swelling in polyelectrolyte gels*, J. Chem. Phys., 93 (1990), 4462, https://doi.org/10.1063/1.458729.
[15] J. K. Hale, *Ordinary Differential Equations*, 2nd ed., Robert E. Krieger, Huntington, NY, 1980.
[16] S. Hirotsu, *Static and time-dependent properties of polymer gels around the volume phase transition*, Phase Transitions, 47 (1994), pp. 183–240, https://doi.org/10.1080/01411599408200347.
[17] M. W. Hirsh, *Systems of differential equations which are competitive or cooperative:* I. *Limit sets*, SIAM J. Math. Anal., 13 (1982), pp. 167–179, https://doi.org/10.1137/0513013.
[18] M. W. Hirsh, *Systems of differential equations which are competitive or cooperative:* I. *Convergence almost everywhere*, SIAM J. Math. Anal., 16 (1985), pp. 423–439, https://doi.org/10.1137/0516030.
[19] M. W. Hirsh, *Systems of differential equations which are competitive or cooperative:* IV. *Structural stability in three-dimensional systems*, SIAM J. Math. Anal., 21 (1990), pp. 1225–1234, https://doi.org/10.1137/0521067.
[20] A. Katchalsky, *Polyelectrolyte gels*, Progress in Biophysics and Biophysical Chemistry, 4 (1954), pp. 1–59.
[21] J. P. F. Lagerwall and G. Scalia, *A new era for liquid crystal research: Applications of liquid crystals in soft matter nano-, bio- and microtechnology*, Curr. Appl. Phys., 12 (2012), pp. 1387–1412, https://doi.org/10.1016/j.cap.2012.03.019.
[22] O. D. Lavrentovich, *Transport of particles in liquid crystals*, Soft Matter, 10 (2014), pp. 1264–1283, https://doi.org/10.1039/C3SM51628H.
[23] P. Leenheer and H. L. Smith, *Virus dynamics: A global analysis*, SIAM J. Appl. Math., 63 (2003), pp. 1313–1327, https://doi.org/10.1137/S0036139902406905.
[24] B. Li and R. A. Siegel, *Global analysis of a model pulsing drug delivery oscillator based on chemomechanical feedback with hysteresis*, Chaos, 10 (2000), pp. 682–690, https://doi.org/10.1063/1.1286998.
[25] H. F. Mark and J. I. Kroschwitz, *Encyclopedia of Polymer Science and Engineering*, 2nd ed., Wiley, New York, 1985.
[26] G. P. Misra and R. A. Siegel, *New mode of drug delivery: Long term autonomous rhythmic hormone release across a hydrogel membrane*, J. Control. Release, 81 (2002), pp. 1–6, https://doi.org/10.1016/S0168-3659(02)00043-3.
[27] B. Peng, V. Gaspar, and K. Schwalter, *False bifurcations in chemical systems*, Phil. Trans. Royal Soc. A, 337 (1991), pp. 275–289, https://doi.org/10.1098/rsta.1991.0123.
[28] N. A. Peppas, *Hydrogels in Medicine and Pharmacy*, CRC Press, Boca Raton, FL, 1986.

[29] J. Ricka and T. Tanaka, *Swelling of ionic gels: Quantitative performance of the Donnan theory*, Macromolecules, 17 (1984), pp. 2916–2921, https://doi.org/10.1021/ma00142a081.
[30] J. Siepmann, R. Siegel, and M. Rathbone, eds., *Fundamentals and Applications of Controlled Release Drug Delivery*, Springer, New York, 2012, https://doi.org/10.1007/978-1-4614-0881-9.
[31] H. L. Smith, *Monotone Dynamical Systems*, Math. Surveys Monogr. 41, AMS, Providence, RI, 1995.
[32] Y. Song, X. Chen, V. Dabade, T. W. Shield, and R. D. James, *Enhanced reversibility and unusual microstructure of a phase-transforming material*, Nature, 502 (2013), pp. 85–88.
[33] H. Yasuda, C. E. Lamaze, and A. Peterlin, *Diffusion and hydraulic permeabilities of water in water-swollen polymer membranes*, J. Polym. Sci. B Polym. Phys., 9 (1971), pp. 1117–1131, https://doi.org/10.1002/pol.1971.160090608.
[34] H. Yasuda, C. E. Lamaze, and A. Schindler, *Salt rejection by polymer membranes in reverse osmosis.* II. *Ionic polymers*, J. Polym. Sci. B Polym. Phys., 9 (1971), pp. 1579–1590, https://doi.org/10.1002/pol.1971.160090903.